

2. EXPLANATORY NOTES¹

Shipboard Scientific Party²

INTRODUCTION

In this chapter, we have assembled information that will help the reader understand the basis for our preliminary conclusions and help the interested investigator select samples for further analysis. This information concerns only shipboard operations and analyses described in the site reports in the *Initial Reports* volume of the Leg 176 *Proceedings of the Ocean Drilling Program*. Methods used by various investigators for shore-based analyses of Leg 176 data will be described in the individual scientific contributions published in the *Scientific Results* volume and in publications in various professional journals.

Authorship of Site Chapter

The separate sections of the site chapter were written by the following shipboard scientists (authors are listed in alphabetical order, no seniority is implied):

Leg Summary: Dick, Natland

Operations: Dick, Miller, Natland, Storms

Igneous Petrology: Holm, Le Roux, Maeda, Meyer, Naslund, Natland, Niu, Snow

Metamorphic Petrology: Alt, Bach, Bideau, Kelley, Robinson

Geochemistry: Hertogen

Structural Geology: Hirth, Ildefonse, John, Trimby, Yoshinobu

Paleomagnetism: Gee, Kikawa, Worm

Physical Properties: Kingdon, Stephen

Downhole Logging: Haggas, Iturrino, Kingdon, Stephen, Worm

Shore-based Logging: Bartetzko

Visual Core Description: Shipboard Scientific Party

¹Examples of how to reference the whole or part of this volume.

²Shipboard Scientific Party addresses.

Numbering of Sites, Holes, Cores, and Samples

Drilling sites are numbered consecutively from the first site drilled by the *Glomar Challenger* in 1968. A site refers to one or more holes drilled while the ship was positioned over a single acoustic beacon. Multiple holes are often drilled at a single site by pulling the drill pipe above the seafloor (out of the hole), offsetting the ship some distance from the previous hole (without deploying a new acoustic beacon), and drilling another hole.

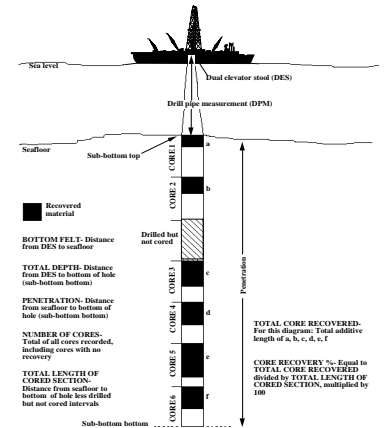
For all Ocean Drilling Program (ODP) drill sites, a letter suffix distinguishes each hole drilled at a single site. The first hole at a given site is assigned the suffix A, the second hole is designated with the same site number and assigned suffix B, and so on. Note that this procedure differs slightly from that used by the Deep Sea Drilling Project (DSDP; Sites 1–624) but prevents ambiguity between site- and hole-number designations. These suffixes are assigned regardless of recovery, as long as penetration takes place. Distinguishing among holes drilled at a site is important, because recovered rocks from different holes, particularly when recovery is less than 100%, are likely to represent different intervals in the cored section.

The cored interval is measured in meters below seafloor (mbsf); sub-bottom depths assigned to individual cores are determined by subtracting the drill-pipe measurement (DPM) water depth (the length of pipe from the rig floor to the seafloor) from the total DPM (from the rig floor to the bottom of the hole; see Fig. F1). Water depths below sea level are determined by subtracting the height of the rig floor above sea level from the DPM water depth. The depth interval assigned to an individual core begins with the depth below the seafloor at which the coring operation began and extends to the depth that the coring operation ended for that core (see Fig. F1). Each coring interval is equal to the length of the joint of drill pipe added for that interval (~9.4 to 10.0 m). The pipe is measured as it is added to the drill string, and the cored interval is usually recorded as the length of the pipe joint to the nearest 0.1 m. However, coring intervals may be shorter and may not be adjacent if separated by intervals drilled but not cored or washed intervals.

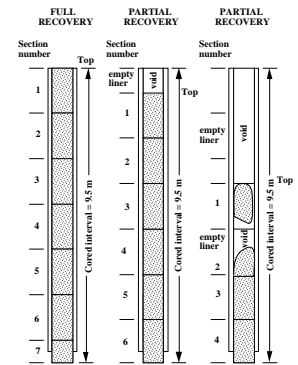
Cores taken from a hole are numbered serially from the top of the hole downward. Core numbers and their associated cored intervals (in mbsf) are usually unique in a given hole; however, this may not be true if an interval must be cored twice, because of caving of cuttings or other hole problems. The maximum full recovery for a single hard-rock core is nominally 9.5 m of rock contained in a core barrel (5.6–5.8 cm diameter; Fig. F2). Recovery >100% may occur, however, where core drilled was not fully recovered from the previous interval. Only rotary coring barrel bits were used during Leg 176.

Because of core-jamming in liners, nearly all cores recovered during Leg 176 were collected without core liners. The pieces of the core were pulled from the bottom of the core barrel. The bottoms of oriented pieces (i.e., pieces that clearly could not have rotated about a horizontal axis in the core barrel) were marked with a red wax pencil to preserve orientation during the splitting and labeling process. The pieces were transferred to a 1.5-m-long split core liner for handling. Contiguous fragments with obvious features allowing realignment were considered to be a single piece. Plastic spacers were used to separate the pieces. Each piece was numbered sequentially from the top of each section, beginning with number 1; reconstructed groups of pieces were lettered consecutively (e.g., 1A, 1B, 1C, etc.; see Fig. F3). Pieces were labeled on

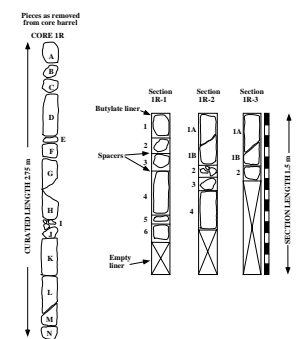
F1. Coring operations and core recovery terms, p. 28.



F2. Hard-rock core division procedure, p. 29.



F3. Core curation procedures for hard rocks, p. 30.



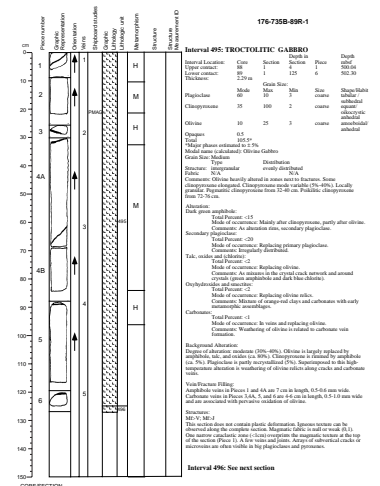
external surfaces, and, if oriented, a this-way-up arrow was added to the label.

Recovery rates were calculated based on the total length of a core recovered divided by the length of the cored interval (see Fig. F1). As most hard-rock coring operations are characterized by <100% recovery, the spacers between pieces can represent intervals of no recovery up to the difference in length between a cored interval and the total core recovered. Of the more than 120 cores recovered during Leg 176, 18 had a curated length in excess of the cored interval. While this is not unique when sampling sediments (gas expansion in the core liners causes anomalously high curated core lengths), it is problematic when dealing with curation of hard-rock cores (which do not expand). In 15 of the 18 circumstances, the error is <5% and is almost certainly caused by misestimation of the depth of penetration at the rig floor. During most of the Leg 176 operations, rig floor heave was >2 m; error of 20-30 cm in depth of penetration yields 2-3% error in recovery calculations. In all other cases, the incidence of high recovery was immediately preceded by a lower recovery core. Amount of unrecovered core in the previous cored interval was invariably greater than the amount of material oversampled and was likely caused by a piston of rock that was left behind as a core barrel was retrieved, only to be picked up on the subsequent coring run. Since the database was not designed to process cores starting at a level above the depth of penetration of the previous core, we could not make this correction to archived data. The interested reader should be aware of these anomalies, however, and account for these discrepancies when using curated length or recovery data. All cores recovered during Leg 176 were designated "R" (rotary drilled) for curatorial purposes. For detailed descriptions of each core sampled, including photographs of each core, and for thin-section descriptions, see the "Core Descriptions" contents list. Also included on this CD-ROM are logs that list details of Leg 176 photomicrographs (see "Photomicrographs" contents list).

Summary Core Descriptions

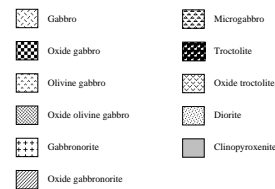
As an aid to the interested investigator, we have compiled summary information of core descriptions on a section-by-section basis and presented these on hard-rock visual core description (HRVCD) forms (see the "Core Descriptions" contents list). These forms summarize the igneous, metamorphic, and structural character of the core, and present graphical representations of the pieces recovered and the lithologic units identified (see Fig. F4). The far right side of these forms presents an image of the archive half of the core captured shortly after splitting. To the right side of the image, several columns contain information about the core. In left-to-right sequence, these columns include archived piece numbers and a graphic representation of piece shape with additional details (veins, fractures, etc.) added to help distinguish features in the image. Next to these is a column indicating pieces that could be oriented relative to the core top and a vein number column for correlation with a vein log (see "Metamorphic Petrology," p. 10). The next column indicates the location of shipboard samples. For reference, the samples noted conform to the sampling code in the JANUS database (XRF = X-ray fluorescence analysis; TSB = polished thin-section billet; PMAG = paleomagnetic samples, most of which were passed to the physical properties laboratory; and XRD = X-ray diffraction analysis). A graphic lithology column illustrates changes in lithologic units (see

F4. Example of hard-rock VCD form, p. 31.



“Igneous Petrology,” p. 4); lithologies recovered are represented by the patterns illustrated in Figure F5. A unit number corresponds to each lithologic unit and is recorded in the next column. Metamorphic intensity intervals are represented by uppercase letters (see “Metamorphic Petrology,” p. 10). We also present a graphic representation of structural features in the core and a column noting particular structural features (see “Structural Geology,” p. 13). On the right side of these forms is a text summary of observations from each section. The upper and lower contacts of each lithologic interval are noted, as are primary lithology and other comments summarized from igneous descriptions. Text summaries of metamorphic and structural description for each section are also compiled on these forms.

F5. Graphic lithology patterns used, p. 32.



IGNEOUS PETROLOGY

General Procedures

Procedures used during Leg 176 for describing igneous rocks in general follow the outline presented in the “Explanatory Notes” chapter of Leg 153 (Shipboard Scientific Party, 1995), and much of the discussion presented here comes from that source. Observations on hard-rock petrology and petrography were stored in ODP written and electronic media and in Excel spreadsheet files according to the definitions given below and the terminology and outlines described in “Linked Spreadsheets,” p. 8. For a detailed discussion of the hard-rock core “barrel sheets,” the reader is referred to “Introduction,” p. 1. Hard-rock macroscopic observations of igneous rocks were recorded on HRVCD forms by the igneous petrologists.

Measurements were not made in traditional ODP shift mode but were performed by the entire igneous petrology group working in tandem. For consistency in the measurements, qualitative measurements (especially the selection of igneous contacts) were made by the entire group. Each quantitative measurement (e.g., grain size, mode, etc.) was measured by a single team member through the entire core. This, we believe, resulted in a better and more consistent measurement of macroscopic features than is possible by teams working in shifts.

Igneous units were defined on the basis of primary igneous lithologies and textures. Mineral modes were estimated (each mineral by an independent observer), totaled, and rechecked if the total was not $100\% \pm 10\%$. Plagioclase and augite were estimated to $\pm 5\%$. Because the abundance of each mineral was determined independently, there is no constraint that would require a total of 100% for the mode, as would be the case if a single observer estimated the abundance of all the minerals. Inasmuch as the total derived by this method provides an indication of the accuracy of the method, the modes were not arbitrarily renormalized to 100%. Mineral habits, igneous structures, and igneous fabrics were also recorded, as well as the nature of igneous contacts. Observations were recorded in Excel spreadsheets for each lithologic unit in the core. Details of the individual measurements are given below.

Differences between Leg 176 and Leg 118 VCDs

Differences in the procedures used during Legs 118 and 176, and the opportunity to incorporate insights into the geology of Hole 735B

gained on the earlier leg, have resulted in significant differences in the presentation of the macroscopic visual core descriptions (VCDs) of Leg 176. The Leg 118 report recognized only six major lithotectonic units in the Hole 735B core. A subsequent redescription of the core divided these units into 495 primary igneous lithologic intervals (Dick et al., 1991b). The description of the core during Leg 176 extended the philosophy of that later study, but the larger group involved in the description enabled a more extensive set of measurements to be made.

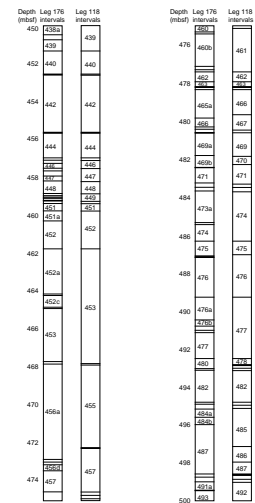
To provide some continuity between these three studies, the lower 50 m of the Leg 118 core from Hole 735B was redescribed using the new system. This is illustrated in Figure F6, where the interval sequences derived by the two data sets are shown side by side. As much as possible the old interval numbers were retained in the new description. Where old intervals were subdivided by the new description, they were labeled A, B, C, and so forth. Where old units were not recognized in the new description, the interval numbers of the old description were skipped in the new sequence.

Rock Classification

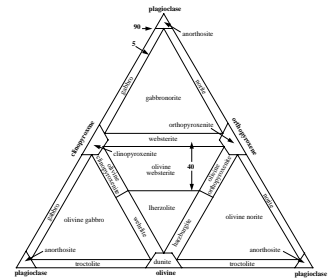
The classification of mafic phaneritic rocks recovered during Leg 176 closely follows the International Union of Geological Sciences (IUGS) system (Streckeisen, 1974; Le Maitre, 1989; Figs. F7, F8). Minor modifications were made to subdivide the rock types more accurately in the Hole 735B core on the basis of significant differences rather than arbitrary cutoffs based on the abundance of a single mineral. For gabbroic rocks, the modifier “disseminated oxide” is used when the abundance of Fe-Ti oxide is 1%–2%, and the modifier “oxide” is used when the abundance is >2%. The terms “orthopyroxene-bearing gabbro” and “gabbronorite” are used to denote the presence of discrete orthopyroxene grains; orthopyroxene present as reaction rims is ignored for the purpose of assigning a rock name. Rocks with between 1% and 5% orthopyroxene are called orthopyroxene-bearing gabbros and samples with >5% orthopyroxene are called gabbronorite. The term “troctolitic” is used to describe olivine gabbros with 5%–15% clinopyroxene and the rock name “troctolite” is used for rocks with <5% clinopyroxene. “Anorthositic” is used for gabbros with >80% plagioclase. High proportions (>65%) of mafic minerals are noted by the prefix mela-, and high proportions (>65%) of plagioclase are noted by the prefix leuco-. The modifier “micro” is used to distinguish gabbroic rocks with a dominant grain size of <1 mm (e.g., microgabbro, microtroctolite, and microgabbronorite). Leucocratic rocks with >20% quartz and <1% K-feldspar (a restricted part of the “tonalite” field of the IUGS system) are called “trondhjemites” in keeping with previous usage in the ocean crust literature. On the HRVCDs, the rock names as described above are given at the top of each interval description, the official IUGS names calculated from the mode are given in the text.

If a mafic rock exhibits the effects of dynamic metamorphism such that the assemblage consists of secondary hydrous minerals that completely obliterate the protolith mineralogy and texture, or if the rock is made up of recrystallized primary minerals such that the original igneous protolith cannot be recognized, the appropriate metamorphic rock names are used. The textural terms “mylonitic,” “schistose,” and “gneissic” are added to metamorphic rock names, such as “greenstone,” “amphibolite,” or “metagabbro” to indicate that the rocks exhibit the effects of dynamic metamorphism. The methods for describing the

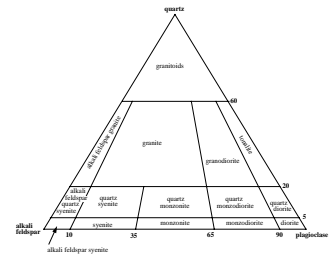
F6. Legs 176, 118 lithostratigraphic intervals compared, p. 33.



F7. Classification of ultramafic and gabbroic rocks, p. 34.



F8. Classification of silicic plutonic rocks, p. 35.



metamorphic and structural petrology of the core are outlined in subsequent sections of this chapter.

Primary Silicate Minerals

The principal rock-forming silicate minerals in the core are plagioclase, olivine, clinopyroxene, and orthopyroxene. For each of these minerals, the following data were recorded in the HRVCDs and in Excel spreadsheets: (1) estimated modal percent of the primary minerals; (2) smallest and largest size of mineral grains (measured along the longest axis in millimeters); (3) average crystal size for each mineral phase using fine-grained (<1 mm), medium-grained (1–5 mm), coarse-grained (5–30 mm), and pegmatitic (>30 mm); (4) mineral shapes using terms such as equidimensional, tabular, prismatic, platy, elongate, acicular, and amoeboidal; (5) mineral habit using the terms euhedral, subhedral, anhedral, rounded, deformed, and fractured; and (6) mineral occurrence if minerals occurred as chadacrysts or oikocrysts.

Primary Fe-Ti Oxide and Sulfide Mineralogy

The abundance of oxides in the core was visually estimated using a binocular microscope with 10× magnification. A continuous log of oxide abundance was compiled along with average abundances in each interval. Oxide habits in hand sample are divided into the following categories: disseminated, interstitial network, concordant seams, discordant seams, and matrix. There is a strong correlation between the textures and abundance. “Disseminated” is used to describe scattered grains or grain clusters of oxides with no pronounced fabric, and is most commonly observed in samples with low oxide abundances. “Interstitial network texture” is used to describe oxides that occur interstitial to the silicates, surrounding or partially surrounding groups of silicate grains, and was most commonly observed in samples with low to moderate oxide abundances. “Concordant seams” is used to describe thin, elongate lenses or patches of oxides parallel to the silicate fabric, and “discordant seams” is used to describe those that crosscut the silicate fabric. Both types of seams are most commonly observed in samples with low to moderate oxide abundances. “Matrix” is used to describe continuous networks of oxides that completely surround and separate the silicate phases and is most commonly observed in samples with high oxide abundances. Oxide shapes in hand sample are divided into the following categories: euhedral, anhedral, angular aggregates, amoeboidal aggregates, and interstitial lenses. “Euhedral” and “anhedral” are used when it appeared that isolated individual grains were present; “aggregates” are used to describe what appeared to be contiguous grain clusters.

Relative sulfide abundance in hand specimen was estimated using a 10× binocular microscope and a scale of 0 to 5, where 0 = not observed, 1 = rare, 2 = average, 3 = above average, 4 = abundant, and 5 = very abundant. Many samples contain sulfide grains too small to be seen on the saw-cut surface at 10× magnification, and for these samples the estimated abundances are too low. Sulfide habits in hand specimen are divided into the following categories: disseminated, disseminated with oxides, disseminated in silicates, concordant seams, discordant seams, clusters with oxides, clusters in silicates, and massive. “Disseminated in silicates” is used to describe low concentrations of scattered sulfide grains enclosed in silicates, and “disseminated with oxides” is used to

describe low concentrations of scattered sulfide grains enclosed in either silicates or oxides but associated with oxide concentrations. "Concordant seams" is used to describe thin, elongate lenses or patches of sulfides parallel to the silicate fabric, and "discordant seams" is used to describe thin, elongate lenses or patches of sulfides that crosscut the silicate fabric. "Clusters in silicates" is used to describe sulfide grains that are present near other sulfide grains, and are included in silicates, and "clusters with oxides" is used to describe sulfide grains that are present near other sulfide grains included in either silicates or oxides but associated with oxide concentrations. Massive is used to describe large patches or lenses of sulfides with an average dimension >1 cm. Sulfide shapes in hand sample were divided into the following categories: euhedral, anhedral, globular inclusions, angular inclusions, globular interstitial, and angular interstitial. "Euhedral" and "anhedral" are used when isolated individual grains are present; "globular" and "angular" are used to describe what appear to be contiguous grain clusters that are nearly spherical masses or are not nearly spherical, respectively.

Igneous Textures

Textures of igneous rocks are characterized on the basis of grain size, grain shape, preferred mineral orientation, and mineral proportions. The dominant grain size for each unit is recorded as fine grained (<1 mm), medium grained (1–5 mm), coarse grained (5–30 mm), or pegmatitic (>30 mm). Rock textures such as "equigranular," "inequigranular," "intergranular," and "granular" are used to describe the overall texture of each lithologic unit. "Poikilitic," "ophitic," and "subophitic" textures are distinguished according to the predominant grain shapes in each unit. Igneous fabrics that are distinguished include "lamination" for rocks exhibiting a preferred orientation of mineral grains that was likely derived from magmatic processes, "clusters" for mineral aggregates, and "schlieren" for lenses of igneous minerals.

Igneous Structures

Igneous structures noted in the core description include layering, gradational grain-size variations, gradational modal variations, gradational textural variations, and breccias. "Layering" is used to describe planar changes in grain-size, mode, or texture within a unit. Grain-size variations are described as normal if the coarser part was at the bottom and as reversed if the coarser part was at the top. Modal variations are described as normal if mafic minerals are more abundant at the bottom and as reversed if mafic minerals are more abundant at the top. "Igneous breccia" is noted where the breccia matrix appears to be of magmatic origin.

Contacts between Lithologic Intervals

The most common types of contacts are those without chilled margins. These are either planar, curved, irregular, interpenetrative, sutured, or gradational. Sutured refers to contacts where individual mineral grains are interlocking across the contact. In many cases, contacts are obscured by subsolidus or subgravidus deformation and metamorphism and are called "sheared" if an interval with deformation fabric is in contact with an undeformed interval, "foliated" if both

intervals have deformation fabrics, or “tectonic” if the contact appears to be the result of faulting.

Thin-Section Description

Thin sections of igneous rocks were examined to complement and refine the hand-specimen observations. In general, the same type of data were collected from thin sections as from hand-specimen descriptions, and a similar terminology is used. Modal data were collected using standard point-counting techniques. All data are recorded in the thin-section spreadsheet (see “[Appendix](#),” p. 31, in the “Leg 176 Summary” chapter) and summarized in ODP-format thin-section descriptions (see the “[Core Descriptions](#)” contents list). Crystal sizes were measured using a micrometer scale and are generally more precise than hand-specimen estimates. The presence of inclusions, overgrowths, and zonation is noted, and the apparent order of crystallization is suggested in the comment section for samples with appropriate textural relationships. The presence and relative abundance of accessory minerals such as oxides, sulfides, apatite, and zircon are noted. The percentage of alteration is also reported (see “[Metamorphic Petrology](#),” p. 10).

Linked Spreadsheets

Because the hard-rock application of JANUS was not yet complete, and the old database (HARVI) had been discontinued, igneous data collected during this leg are recorded in a set of linked Microsoft Excel spreadsheets. There are five interlinked spreadsheets ([I_LITH.XLS](#), [I_TEX.XLS](#), [I_MIN.XLS](#), [I_COMM.XLS](#), and [DEPTH.XLS](#)) and three independent spreadsheets ([I_OPAQUE.XLS](#), [I_VEIN.XLS](#), and [176GEOCH.XLS](#)) in this collection (For detailed information on the spreadsheets, see “[Appendix](#),” p. 31, in the “Leg 176 Summary” chapter). The interlinked spreadsheets cover lithologies, mineralogy, textures, and comments. Most data in these spreadsheets are recorded as numerical values, and the numeric codes are translated to English and back via a pair of “Visual Basic for Applications” (VBA) look-up macros. Information about igneous contacts is recorded in the lithology spreadsheet ([I_LITH.XLS](#)). This includes information about the position of the contact, its depth, the thickness and type of rock above the contact, the type of contact (e.g., igneous or tectonic), and the form of the contact (e.g., planar or curved).

The other three databases link to the [I_LITH.XLS](#) spreadsheet columns defining the position of the lower contact of each interval. The [I_MIN.XLS](#) spreadsheet additionally records the mode of the igneous minerals (plagioclase, clinopyroxene, olivine, orthopyroxene, oxides, and sulfides), as well as the grain size of the silicate minerals (plagioclase, clinopyroxene, olivine, and orthopyroxene). From these data, a rock name is automatically generated by a VBA macro. The [I_TEX.XLS](#) spreadsheet records mineral shapes (e.g., acicular, platy, etc.) and habits (e.g., chadacrystic, ophitic, etc.). The [I_COMM.XLS](#) spreadsheet contains number codes for igneous textures and fabrics, as well as text comments on each interval. An independent (unlinked) spreadsheet, [I_OPAQUE.XLS](#), records the approximate oxide abundance in the recovered core on a centimeter by centimeter basis.

An independent (unlinked) spreadsheet, [I_VEIN.XLS](#), records the data on “trondhjemite veins.” Here, “trondhjemite” represents any of the various quartzo-feldspathic igneous rocks that were recovered

Note: To open the Excel spreadsheets, either click on the file-names in the text or open the files through Microsoft Excel. To use the in-text links, your computer must be configured to automatically launch Microsoft Excel when files with .XLS extensions are opened. The spreadsheet files can be found in the
\\176_IR\SUPP_MAT\
APPENDIX\ directory on the CD-ROM.

(including tonalite and granodiorite), it being the most common. Trondhjemite of apparent igneous origin that crosscuts the core, and that is more than 5 cm in thickness along the length of the core, is recorded as a separate lithologic interval. Trondhjemite of igneous or hydrothermal origin that is less than 5 cm in thickness along the length of the core is recorded as a vein. Although this is an arbitrary cutoff, it provides a workable solution for the description of the hundreds of thin trondhjemite dikelets, fracture fillings, and/or veins that cut the core. The [I_VEIN.XLS](#) spreadsheet records the position and igneous interval of each trondhjemite vein, the apparent thickness relative to the vertical axis of the core, the true thickness perpendicular to the plane of the vein, the thickness of the zone in which the vein or vein network occurs, the percentage by area of trondhjemite within that zone, and comments about the vein. Although many of the thicker “veins” appear to be of igneous origin, for many of the veins it is not possible in hand specimen to determine whether they are of igneous or hydrothermal origin. Although the log excludes veins of clearly hydrothermal origin, it includes any veins of unclear origin.

A macro in the [I_MIN.XLS](#) file extracts a condensed data report on each igneous interval. This macro is accessed from the “Report” worksheet of the [I_MIN.XLS](#) spreadsheet. All other spreadsheets must first be loaded and translated using their respective “Translate” buttons; then the Up and Down buttons on the report page scroll through the entire database one line at a time. It is possible to jump to any part of the database by typing an interval number in the appropriate cell and pressing the “Go” button. This loads the values from that interval into the report and copies the entire report onto the (Windows or Mac) clipboard.

Multi-interval reports are generated by switching to the “Mineralogy” worksheet and highlighting a group of interval numbers, switching back to the report sheet and pressing the “Multi” button. The corresponding unit reports are formatted and transferred via OLE to Microsoft Word. Word is then brought to the foreground, where further editing can take place.

Depths below seafloor for the igneous spreadsheets and for other purposes are calculated using the EDepth and CDepth functions of the [DEPTH.S.XLS](#) spreadsheet. This spreadsheet by default hides itself after loading. Its functions can be used by selecting the Tools|Add-ins menu item in Excel. From the Add-in manager dialog box select “Browse,” and go to the DPTHSMTH\EXCOM directory where [DEPTH.S.XLS](#) resides. Double click on DEPTH.S.XLA to install this add-in to Excel. If a dialogue box asks you to copy the add-in to the Microsoft Default Library, it is important to select “NO.” The item “Hole 735B Depths” should now be listed as an item in the Add-in manager. It is now permanently installed in Excel until the checkbox next to its name is deselected, which will uninstall it. The depth calculator will now reload automatically every time Excel is started. To use the depth calculator, type in a destination cell

=EDepth(A1,B1,C1/100).

Make sure to replace A1 in this equation with the cell where the core number of interest resides, making sure that the core number is an integer rather than the alphanumeric combination (i.e., 90 instead of 90R). Replace B1 with the cell where the section number of interest resides and C1 with the cell where curated depth in the section resides (in cm).

Note: Add-in functions may not operate in all versions of Microsoft Excel.

Expanded/compressed depth should appear in the destination cell, which can be copied and pasted to subsequent cells.

An additional add-in menu item was also written that calculates a spatial moving average of irregularly spaced data points. This add-in item resides in the DPTHSMTH directory in a subdirectory named SMOOTH. The "Smooth" add-in is installed the same way as the depths calculation add-in (see above). Once the add-in is installed, it adds the item "Smooth" to the Tools menu. To use this function, make sure there is a free column in a destination spreadsheet for the output. Depths and values for those depths must reside in two other columns. Highlight a few cells of the output destination column and select "Smooth" from the tools menu. A "Set-up" dialog box will appear; ensure the destination range is correct. Enter into the cells below the destination range the number of columns that the depth and value range are offset from the output column and select a smoothing interval. Selecting the "Fast" checkbox speeds up the smoothing process by hiding the individual cell updates. The "Keep Going" checkbox instructs the algorithm to keep working its way downward as long as there is data to process. Once everything is entered, selecting the "Go" icon should output smoothed data to the destination column.

Igneous Lithology, Interval Definitions, and Summary

For a complex sequence of plutonic rocks, interpretations of the vertical lithologic successions in the core are difficult because of overprinting of synmagmatic, metamorphic, and tectonic processes. The lithologic intervals adopted here are defined by vertical sections with consistent internal characteristics and lithology and are separated based on geological contacts defined by significant changes in modal mineralogy or primary texture, as encountered downhole. To the extent possible, boundaries were not defined where changes in rock appearance were only the result of changes in the type or degree of metamorphism, or the intensity of deformation. Both sharp and gradational contacts occur between intervals. If the contact was recovered, its location is recorded by the core, section, position (cm), and piece number. If the contact was not recovered, but a significant change in lithology or texture is observed, the contact is placed at the bottom of the lowest piece of the upper interval. The information recorded for each section of the core includes the rock type; igneous, metamorphic, and/or deformational texture; evidence for igneous layering; extent, type, and intensity of deformation; primary, and secondary minerals present; grain shape for each primary mineral phase; evidence of preferred orientation; the position of quartzo-feldspathic veins (whether of igneous or hydrothermal origin); and general comments. The description and summary of each interval were entered into the standard ODP-format program where the general lithologic description and top and bottom of the interval are recorded with reference to curated core, section, piece(s), depth, and thickness.

METAMORPHIC PETROLOGY

Visual core descriptions of metamorphic characteristics were compiled together with igneous and structural documentation of the core to provide information on the extent of alteration, alteration mineral phases, and vein characteristics. These data were recorded in the Alter-

ation and Vein Logs (for detailed information see “Appendix,” p. 31, in the “Leg 176 Summary” chapter [BGALTLOG.XLS, VEINLOG.XLS]), respectively, and are summarized in the HRVCDs. To ensure accurate core descriptions, the petrography of representative samples was recorded in the Alteration Thin-Section Log (see “Appendix,” p. 31, in the “Leg 176 Summary” chapter) and integrated with the visual core descriptions. Identification of mineral phases was checked by XRD analyses according to ODP standard procedures outlined in previous *Initial Reports* volumes (e.g., Volume 118; Shipboard Scientific Party, 1989). For each section the following information was recorded: leg, site, hole, core number, core type, section number, piece number (consecutively downhole), and position in the section.

Macroscopic Descriptions

The metamorphic mineral assemblages and alteration intensity were recorded in the Alteration Log. Primary phases (olivine, clinopyroxene, orthopyroxene, and plagioclase) and the secondary minerals that replace them were noted and, where possible, the volume percent of each phase was estimated in hand specimen and checked by observation of representative thin sections. Vein mineralogy, vein length and width (measured on the cut face of a piece or pieces), the top and the bottom location of the vein in the piece(s), vein type, vein mineralogy and mineral abundance, associated halo widths, and wall rock alteration were recorded in the Vein Log. The length and width of each vein were used to calculate the vein area; where veins are very abundant (net veins), the percent area of the veins within a piece or interval was estimated visually. These data were used to calculate the density of veins in the core and the volume percentage of each vein type within a given interval and within the entire core.

Thin-Section Descriptions

Detailed petrographic descriptions were made aboard ship to aid in identification and characterization of metamorphic and vein mineral assemblages. Stable mineral parageneses were noted, as were textural features of minerals indicating overprinting events (e.g., coronas, overgrowths, and pseudomorphs). Mineral abundances were either estimated visually or determined by point counting. These data are recorded in the Alteration Thin Section Log and summarized in the thin-section descriptions (see the “Core Descriptions” contents list). The modal data allowed accurate characterization of the intensity of metamorphism and aided in establishing the accuracy of the macroscopic and microscopic visual estimates of the extent of alteration.

GEOCHEMISTRY

Samples considered by the shipboard scientific party to be representative of the various lithologies cored were analyzed for major oxide and selected trace element compositions with the shipboard ARL 8420 wavelength-dispersive XRF apparatus. Full details of the shipboard analytical facilities and methods are presented in previous ODP *Initial Reports* volumes (e.g., Legs 118, 140, 147, 153; Shipboard Scientific Party, 1989, 1992, 1993, 1995a). The elements analyzed and the operating conditions for Leg 176 XRF analyses are presented in Table T1.

After coarse crushing, samples were ground in a tungsten carbide shatterbox. Then 600-mg aliquots of ignited rock powder were intimately mixed with a fusion flux consisting of 80 wt% lithiumtetraborate and 20 wt% "heavy absorber" La_2O_3 . The glass disks for the analysis of the major oxides were prepared by melting the mixture in a platinum mold in an electric induction furnace. Trace elements were determined on pressed powder pellets prepared from 5 g of rock powder (dried at 110°C) mixed with a small amount of a polyvinylalcohol binder solution. The calibration of the XRF system was based on the measurement of a set of reference rock powders. A Compton scattering technique was used for matrix absorption correction for trace element analysis.

The total sum of the oxides determined on ignited powders was generally high. About 60% of the samples had "totals" between 101% and 103%. The systematic analytical error presumably reflects small inadequacies in the procedure for correction for matrix absorption or errors in the concentration of the "heavy absorber" in the fusion flux. A small set of samples was reanalyzed after the cruise by atomic emission and atomic absorption spectrometry at Leuven University, Belgium. It appeared that the error affects all the major element oxides, but it significantly affects only the result of the main component SiO_2 , and to lesser extent of Al_2O_3 , CaO , MgO , and Fe_2O_3 .

A second analytical problem concerned the trace element zirconium. Zirconium data for olivine gabbros obtained during Leg 176 were systematically higher than in equivalent rocks analyzed during Leg 118. To determine whether this was a real geochemical difference, a selection of Leg 118 shipboard powder samples was reanalyzed during Leg 176. Consistently higher Zr values were obtained. A postcruise analysis of control samples at the Universities of Copenhagen, Denmark, and Leuven, Belgium, showed that the lower values obtained during Leg 118 are the more accurate ones. Inadequacies in the correction for the interference of Sr X-rays on Zr X-ray peaks are the most likely source of analytical errors. Unfortunately, the problem could not be remedied during the cruise. As a consequence, the reported Zr data may be too high by a factor of two in the 15- to 30-ppm concentration range. At higher Zr concentration levels, the effect of the analytical error is minor.

Loss on ignition (LOI) for each sample was determined by the standard practice of heating an oven-dried (110°C) sample to 1010°C for several hours. To more fully investigate the results of LOI determinations of selected samples, gas chromatography of the expelled volatiles was performed on a Carlo Erba NA 1500 CHS analyzer; 20 mg of dried (110°C) rock sample was combusted at 1010°C , releasing water and carbon dioxide. Sulfur from sulfide minerals is oxidized to SO_2 (by addition of V_2O_5), and SO_3 is released from any sulfate minerals present in the sample. Gas-chromatographic separation was followed by quantitative determination of the respective gaseous oxides of carbon, hydrogen, and sulfur by a thermal conductivity detector. Reagent grade sulfanilamide ($\text{C}_6\text{H}_8\text{N}_2\text{O}_2\text{S}$) was used to calculate the bias factor of the analyzer for CO_2 , H_2O , and SO_3 . Control rock samples covering the concentration ranges of hydrogen, carbon, and sulfur observed in the cored samples were repeatedly analyzed. These control samples were prepared by intimately mixing weighed quantities of a low-sulfur, low-carbon silicate rock (Gaby 153 Interlaboratory Standard prepared during Leg 153) and of sediment sample ODP6 (containing 3.2 wt% C, 0.56 wt% H, and 5300 ppm S). Because the concentration of total sulfur in most of the

rock samples was close to the determination limit of the CHS analyzer, results of duplicate analyses for sulfur showed large scatter. Therefore, no results of sulfur analysis are listed in this volume.

After the cruise all the shipboard samples were analyzed for ferrous iron content at the University of Leuven, Belgium, using the redox-titration method of Shafer (1966). Sample aliquots weighing from 50 to 100 mg were dissolved in a H₂SO₄/HF mixture in a nitrogen atmosphere. Ferrous iron is titrated with potassium-dichromate solution using sodiumdiphenylaminesulfonate as a redox color indicator.

STRUCTURAL GEOLOGY

Conventions for structural studies established during previous “hard-rock” drilling legs (e.g., Legs 118, 131, 140, 147, and 153) were generally followed during Leg 176. However, several minor changes in nomenclature and procedure were adopted. These changes are described below. Where procedures followed directly from previous legs, references to the appropriate *Initial Reports* “Explanatory Notes” chapter are given.

Overview of Macroscopic Core Description

Because of the high recovery rate during Leg 176, archive halves of the cores were stored immediately, and all structural measurements had to be made on the working halves. Following procedures described in the Leg 153 *Initial Reports* volume (Shipboard Scientific Party, 1995a), data were entered into a VCD form (Fig. F4), used in conjunction with five spreadsheet logs (see “Appendix,” p. 31, in the “Leg 176 Summary” chapter). The structural sketches drawn on the VCD form are intended to illustrate the most representative structures and crosscutting relationships present on a core section; in addition, a brief general description of the structures is printed on the same form. Where no magmatic fabric, or only a weak one, was present (predating any other structure), the structural column was left blank.

Paper copies of spreadsheet forms were used for recording specific structures and measurements during core description. Separate spreadsheets were used to record data on (1) joints, veins, cleavage, and folds; (2) breccias, faults, and cataclastic fabrics; (3) crystal-plastic fabrics and sense of shear indicators; (4) magmatic fabrics, compositional layering, and igneous contacts; and (5) crosscutting relationships. The description and orientation of all features were recorded using curated depth so that “structural intervals” could be correlated with other lithologic intervals. The spreadsheets were organized to identify five separate types of structural intervals using deformation intensity scales summarized in Table T2. The structural geologists worked together during the same shift to minimize measurement inconsistencies. Each member of the team was responsible for making a specific set of observations throughout the entire core (e.g., characterization of magmatic fabric intensity). Descriptions and structural measurements were based on observations on the working half of the core (see orientation of structures below).

T2. Deformation intensity scales,
p. 40.

Nomenclature

To maintain consistency of core descriptions, we used feature “identifiers” for structures similar to those outlined in Shipboard Scientific Party (1995a). Modifications to this scheme are shown in the comments checklist (Table T3) and include designation of breccia type (hydrothermal - Bh, cataclastic - Bc, or magmatic - Bm). In core sections where crystal-plastic fabrics clearly overprint brittle hydrothermal or magmatic breccia, a note was made in the comment section of the crystal-plastic fabric spreadsheet that deformation occurred in the retrograde metamorphic assemblage. Where brittle fabrics overprint crystal-plastic fabrics, or deformation was “semi-brittle,” a note was made in the comments section and documented in the crosscutting relations spreadsheet.

Structural Measurements

Structural features were recorded relative to core section depths in centimeters from the top of the core section. Depth was defined as the point where the structure intersects the center of the cut face of the working half of the core, as detailed during Leg 153 (see fig. 15A in Shipboard Scientific Party, 1995a). Crosscutting relationships were described in intervals delimited by top and bottom depth.

Apparent fault displacements were recorded as they appeared on the cut face of the archive half of the core and the end of broken pieces. Displacements seen on the core face were treated as components of dip-slip movement, either normal or reverse. Strike-slip displacements of vertical features were termed either sinistral or dextral. Displacements of features visible on the upper and lower surfaces of core pieces were treated as components of strike slip and termed sinistral or dextral. Displacements were measured between displaced planar markers, parallel to the trace of the fault. Additional cuts and slickenside orientations were incorporated wherever possible to differentiate among apparent dip slip, oblique slip, and strike slip.

The structures were oriented with respect to the core reference frame; the convention we used for the core reference frame is explained in Shipboard Scientific Party (1995a) and shown at the top of the comments box in the structural data spreadsheets (see “Appendix,” p. 31, in the “Leg 176 Summary” chapter).

Planar structures were oriented using the techniques outlined during Legs 131 and 153 (Shipboard Scientific Party, 1991; 1995a). Apparent-dip angles of planar features were measured on the cut face of the working half of the core. To obtain a true-dip value, a second apparent-dip reading was obtained where possible in a section perpendicular to the core face (second apparent orientation). Apparent dips in the cut plane of the working core were recorded as two-digit numbers (between 00° and 90°) with a dip direction to 090° or 270°. In the “second” plane, apparent-dip directions were recorded as either 000° or 180°. The dip and the dip direction with respect to the working half of the core were recorded on the spreadsheet together with second plane measurements. If the feature intersected the upper or lower surface of the core piece, measurements were made directly of the strike and dip in the core reference frame. Where broken surfaces exposed lineations or striations, the trend and plunge were measured directly, relative to the core reference frame.

T3. Checklist used for spreadsheet comments, p. 41.

The two apparent dips and dip directions measured for each planar feature were used to calculate a true dip. These calculations were performed using either (1) LinesToPlane by S.D. Hurst or (2) App2truedip by B. Celerier (see “Appendix,” p. 31, in the “Leg 176 Summary” chapter). Calculated data can be read directly into the shareware stereonet plotting program Stereoplot 3.05 of Neil Mancktelow.

Deformation Intensities

A semiquantitative scale of deformation intensities was used by the shipboard structural geologists during core description. This scale, shown in Table T2, has been modified from the deformation scale used during Leg 147 (table 2 in Shipboard Scientific Party, 1993) and the fabric intensity scales used during Leg 153 (fig. 13 in Shipboard Scientific Party, 1995a) and conforms to the scales for deformation textures used by Cannat et al. (1991) and Dick et al. (1991b) in the Leg 118 *Scientific Results* volume. Wherever possible we have assigned specific values to intensity estimates (e.g., the spacing of veins; the percentage of matrix in a cataclastic zone) to maintain consistency throughout the core. However, for some categories this proved difficult (e.g., the intensity of any crystal-plastic fabric) in which cases we have used qualitative estimates of intensity based on hand-specimen and thin-section observations. We chose five distinct types of deformation for intensity measurements (Table T2):

1. Magmatic: The presence and intensity of any shape-preferred orientation of magmatic phases. Four levels, from no shape-preferred orientation (0) to a strong shape-preferred orientation (3), were used.
2. Crystal-plastic: Six levels of deformation intensity were used, ranging from a lack of any crystal-plastic fabric, through two stages of foliation development, and finally to (ultra)mylonitic fabrics.
3. Cataclastic: Six levels of deformation intensity were used with fabrics categorized depending on the percentage of matrix present within each cataclastic zone. Thin-section descriptions, wherever possible, significantly aid this categorization.
4. Joints (fractures): Four levels of joint density were used, depending on the average frequency of joints across a 10-cm depth interval along the long axis of the core. Joints were distinguished from faults (cataclastic features) by the lack of any identifiable offset.
5. Veins: The same four-level scale of density used for joints was incorporated for veins. However, where there was an identifiable offset across a vein, it was treated as a fault rather than a vein. The widths of individual veins were measured by the metamorphic team and entered into the vein log.

Occasionally it proved difficult to differentiate between crystal-plastic and cataclastic deformation in relatively high-strain shear zones based on hand-specimen observations only. For this reason, as during Leg 147, we have tried to classify both of these deformation styles using parallel scales where a certain intensity of cataclasite is a direct equivalent to the same intensity of crystal-plastic deformation.

Initial inspections of the core indicated a prevalence of small, sub-horizontal microfractures throughout the core; to avoid unnecessary

Note: Stereoplot only works on Macintosh computers running OS version 8.1 or lower.

measurements of these regular features, a column was introduced into the structural spreadsheet to indicate the density of these features using the same density scale as for joints. The microfractures, which were likely induced by drilling, have been termed “subhorizontal microfractures” (SHM).

Thin-Section Descriptions

Thin sections were examined to characterize the microstructural aspects of important mesoscopic structures in the core. Classes of information that were obtained include deformation mechanisms on a mineral-by-mineral basis, kinematic indicators, crystallographic and shape fabrics, qualitative estimates of the degree of crystallographic preferred orientation along local, principal finite strain axes, syn- and post-kinematic alteration, and the relative timing of microstructures.

The orientation of thin sections relative to the deformation fabrics and core axes is noted in the comments section of the spreadsheet. Thin sections were oriented, where possible, with respect to the core axis and in the core reference frame described in “[Structural Measurements](#),” p. 14. Selected samples were cut perpendicular to the foliation and parallel to any lineation to examine kinematic indicators and the shape-preferred orientation of minerals (see fig. 15, Shipboard Scientific Party, 1995a). We adopted and modified the thin-section description form used by the structural geologists during Leg 140 (Shipboard Scientific Party, 1992) to enter the microstructural information into the spreadsheet database.

The terms used to describe microstructures generally follow those used during Leg 153. Microstructures of gabbroic rocks recovered at Site 735 are discussed in detail in “[Igneous Petrology](#),” p. 12, and “[Structural Geology](#),” p. 54, in the “Site 735” chapter. Although a large spectrum of microstructures occurs, for the purposes of entering data into spreadsheets a number of textural types characterized by specific microstructural styles were defined and are keyed to the spreadsheet. These are summarized for gabbroic rock in Table [T4](#).

It is possible that superposition of different microstructures or deformation mechanisms may occur during solidification and subsolidus cooling. Thus the physical state of the material during fabric development may span the transition from magmatic to solid state. Fabrics defined entirely by igneous minerals with no crystal-plastic deformation microstructures we term “magmatic.” Where local crystal-plastic fabrics are possibly produced in the presence of melt (e.g., Hirth and Kohlstedt, 1995; Bouchez et al., 1992; Means and Park, 1994; Nicolas and Ildefonse, 1996), we term the physical state “crystal-plastic ± melt.” Where fabric development is produced entirely by dislocation creep, we use the term “crystal-plastic” to define the physical state of the rock. The other groups refer to rocks whose magmatic and/or crystal-plastic texture is overprinted by brittle deformation.

PALEOMAGNETISM

Paleomagnetic measurements were performed on discrete minicore samples and, where practical, on continuous pieces of the archive half-core. A standard 2.5-cm-diameter minicore sample was generally taken from each section of core for shipboard study. Minicore samples were chosen to be representative of the lithology and alteration mineralogy,

T4. Textural types defined for gabbroic rocks, [p. 42](#).

and an effort was made to select samples near important structural features for possible reorientation using the remanent magnetization directions. The azimuths of core samples recovered by rotary drilling are not constrained. All magnetic data are therefore reported relative to the following core coordinates: +X (north) is into the face of the working half of the core, +Y (east) points toward the right side of the face of the working half, and +Z is down (e.g., Leg 153 *Initial Reports* "Explanatory Notes" chapter; Shipboard Scientific Party, 1995a).

The remanent magnetization of continuous core pieces was measured with the 2-G Enterprises (Model 760R) pass-through magnetometer equipped with superconducting quantum interference devices. An in-line alternating field (AF) demagnetizer capable of producing alternating fields up to 80 mT was used with the 2-G magnetometer. The Long Core v2.2 program developed by William Mills was employed. The maximum intensities that could be measured without significant flux jumps remaining depend on the velocity of measurements. Maximum intensities of 7 A/m, corresponding for example to ~20,000 flux counts for a half core measured on the Z sensor, could be measured at the slowest possible tray velocity of 1 cm/s. At 5 cm/s the maximum measurable intensity decreases to ~2 A/m. Archive-half cores were selected for remanence measurements depending on the susceptibility values measured with the multisensor track (MST) whole-core logger. Core pieces having susceptibilities (k) that are >0.05 (SI) were removed from the liner for remanence measurements. The natural remanent magnetization and the remanence remaining after demagnetization (typically at 5, 10, 15, and 20 mT) were measured at an interval of 2 cm.

Oriented discrete samples were obtained as standard 2.54-cm cylindrical samples. These also were measured with the 2-G magnetometer in the discrete sample mode of the Long Core v2.2 program. Because of the reduced volume (10 cm³) compared to half cores, maximum measurable intensities are on the order of 100 A/m. Samples were AF demagnetized up to 80 mT in steps of typically 3, 5, 10, 15, 20, 30, 40, 50, 60, and 80 mT with the integrated demagnetizer. A small number of samples were thermally demagnetized, using the Schönstedt Thermal Demagnetizer (Model TSD-1). The initial susceptibility was monitored between each temperature step as means of assessing mineralogical changes associated with heating.

The anisotropy of magnetic susceptibility was determined for most cylindrical samples, using the Kappabridge KLY-2 and the program ANI20, provided by the manufacturer Geofyzika Brno, Czech Republic. A 15-position measuring scheme is used to derive the susceptibility tensor and associated eigenvectors and eigenvalues.

In addition to standard paleomagnetic measurements, a limited number of discrete samples were given an anhysteretic remanent magnetization (ARM) with a Dtech D-2000 AF Demagnetizer employing peak AF fields of 200 mT and a direct field of 0.1 mT. The ARMs were also measured and AF demagnetized with the 2-G magnetometer.

PHYSICAL PROPERTIES

Introduction

Measurements of the following physical properties were recorded during Leg 176: natural gamma-ray emissions, bulk density (wet and

dry), compressional wave velocity, magnetic susceptibility, thermal conductivity, and electrical resistivity.

Physical properties measurements were performed on the cores in three phases:

1. The whole-core sections (fully intact core in split liners), once equilibrated to laboratory temperatures ($>18^{\circ}\text{C}$), were run through the MST system. This measured three parameters: bulk density, magnetic susceptibility, and natural gamma-ray (NGR) emission. Compressional wave (P -wave) velocity was not recorded using the MST during this leg because of poor acoustic coupling between the liner and core.
2. Following core splitting, thermal conductivity measurements were performed on representative half-round core pieces.
3. Following sampling, the minicores were tested for P -wave velocity, resistivity, and index properties (wet and dry mass and dry volume).

Figure F9 shows a flow diagram of core flow for physical properties measurements for ODP hard-rock boreholes.

F9. Flow chart for physical properties measurements, p. 36.

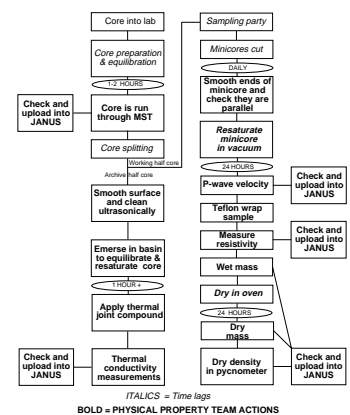
MST Measurements

Bulk Density (Gamma-Ray Attenuation)

The gamma-ray attenuation densiometer (GRAPE) allowed determination of wet bulk density. This was achieved by measuring the attenuation (Compton scattering) of gamma rays passing through the unsplit cores; the degree of attenuation being proportional to natural bulk density (Boyce, 1976; Gerland and Villinger, 1995). The system was calibrated during the cruise using an aluminum density standard. This consisted of four cylinders of varying diameters in a distilled-water-filled core liner; the four different diameters resulted in four different bulk densities. The GRAPE measurements are compromised where the core does not completely fill the core liner, as is the case for all hard-rock cores. Actual measurements were taken at a 4-cm interval, with an integration time of 10 s, and results were output in grams per cubic centimeter.

Magnetic Susceptibility

Whole-core magnetic susceptibility was measured using a Bartington MS2C meter with an 80-mm (internal diameter) loop sensor. Measurements were made at 4-cm intervals, with an integration time of 10 s. The principal controls for the rate of data acquisition of the MST system were the rate of arrival of new core and the acquisition rates of the NGR tool. Longer integration periods could not be chosen because of the limited time available for each measurement. For shipboard analysis, the magnetic susceptibility data were converted to nominal volume-normalized 10^{-5} SI units based on the assumption that the geometric correction factor of 0.66 applied to sediment cores could be used to approximate the correction factor for hard-rock cores.



Natural Gamma-Ray Emission

Natural gamma-ray emission was routinely recorded for all core sections, both to monitor variations in radioactive counts of sample rocks and to provide a correlation with the geophysical logging. The NGR system records radioactive decay of ^{40}K , ^{232}Th , and ^{238}U , three long-period isotopes that decay at an essentially constant rate within measurable time scales. Both the total gamma-ray count and the individual counts from these three isotopes (and therefore their relative contents) were recorded. The installation and operating principles of the NGR system used on board *JOIDES Resolution* are discussed by Hoppie et al. (1994)

The area of influence for the four NGR sensors was about ± 10 cm from the points of measurements along the core axis. As gamma-ray emission is a random event, count times have to be sufficiently large to average for short-period variation. This was achieved on the MST system by utilizing the long area of influence on the sensors and using a moving average window to smooth count rate variations and to achieve a statistically valid sample.

The NGR was calibrated in port against a thorium source. The measurements were made for 10 s every 4 cm, using a twofold moving average window. Results were output in GAPI units for ease of comparability with borehole logging.

Thermal Conductivity

Half-core specimens were nondestructively measured for thermal conductivity using a single-probe Teka (Berlin) TK-04 unit. A half-space needle probe, containing a heater wire and a calibrated thermistor, was clamped onto the flat surface of the half core. Good coupling with the needle probes was ensured by flattening and smoothing the core surface with 240 carbide grit on a glass plate. Thermal conductivity was further improved by the application of a thermally conductive compound between the needle and sample. The samples and needles were then immersed in seawater. This procedure has been used since Leg 140 (Shipboard Scientific Party, 1992), with the TK-04 unit first being used for hard-rock thermal conductivity measurements during Leg 169, and for which full procedures are reported (Shipboard Scientific Party, 1998).

At the beginning of each test, temperatures in the samples were monitored automatically, without applying a heater current, until the background thermal drift was determined to be less than $0.04^\circ\text{C}/\text{min}$. The heater circuit was then closed, and the temperature rise in the probe was recorded.

This technique proved highly sensitive to small variations in ambient temperature. Core samples and monitor needles were therefore equilibrated to a constant temperature by immersion in a covered tank of seawater for at least 1 hr before measurements were taken. In addition, immersion in seawater kept the samples saturated, improved the thermal contact between the needle and the sample, and reduced thermal drift during the tests. Adding a sample or needle to the seawater while the test sample was equilibrating was enough to distort the measurements. Therefore, after any disturbance of the needle or sample, it was left to further equilibrate for at least 15 min to prevent acquisition of erroneous data.

Thermal conductivities were calculated from the rate of temperature rise while the heater current was flowing. The meter was calibrated dur-

ing the cruise against four standards of known thermal conductivity: black rubber, red rubber, basalt, and Macor, which have a similar conductivity range to the tested samples. Temperatures were recorded during a time interval of 80 s, and data were reported in units of $W/(m \cdot K)$.

Compressional (*P*-) Wave Velocities

The pulse transmission method was employed to determine compressional wave velocity. This utilized piezoelectric transducers as sources and detectors in a screw-press modified Hamilton Frame, described by Boyce (1976). All measurements were made on seawater-saturated minicores cut perpendicular to the axis of the core (diameter = 2.54 cm; approximate length = 2 cm) at a confining pressure of zero. A small number of minicores cut parallel to the core axis were also tested.

Minicores for *P*-wave velocity measurements were taken approximately once per core section. The minicores were resaturated with seawater in a vacuum for 24 hr before measurement. Flat ends of the minicores were polished with 240 carbide grit on a glass plate to ensure parallel faces. The length of each minicore was checked using a caliper along its circumference, and grinding continued until all length measurements were within 0.02 mm. Before measurement, the grit was removed by thoroughly cleaning the samples in an ultrasonic bath. Distilled water was used to improve the acoustic contact between the sample and the transducers.

Calibration measurements were performed during the cruise using polycarbonate standard minicores of varying lengths to determine the zero-displacement time delay inherent in the measuring system. Results were recorded in meters per second.

Electrical Resistivity

The electrical resistivity of hard-rock samples was measured on seawater-saturated minicores at room temperature and atmospheric pressure using a two-electrode cell to measure resistance. The method used for derivation of resistivity on board *JOIDES Resolution* was described during Leg 158 (Shipboard Scientific Party, 1995b).

The cell consisted of a nylon holder and spring-loaded aluminum holders. The holder was designed to have the same diameter as the minicores to minimize leakage along the sides of the sample. The measurements were performed with the cylindrical surfaces of the minicores wrapped in Teflon tape to prevent a short circuit between the two ends.

The samples were resaturated in seawater under a vacuum for 24 hr before measurement. The minicore faces were cut smooth and parallel to allow good contact with the electrodes, and seawater was used to ensure good electrical coupling between the electrical contacts and the minicores. The apparatus was calibrated during the cruise against aluminum standard minicores. Because of time constraints, resistivity measurements were made only on a subset of available minicores. Measurements were made at 5 V AC and 50 kHz frequency and were recorded in ohm-meters.

Index Properties

Index properties, as defined for ODP shipboard procedures, were calculated from measurements of wet and dry masses and dry volumes. The sample mass was counterbalanced by a known mass, such that only mass differences of less than 2 g were measured.

Wet mass measurements were made on minicores that were resaturated with seawater in a vacuum for 24 hr. Samples were then oven dried for 24 hr before measurement of dry mass. Volumes were determined using a Quantachrome Penta-Pycnometer, a helium-displacement instrument. The pycnometer measures volumes to a precision of about $\pm 0.005 \text{ cm}^3$, which corresponds to a volume error of 1%. Sample volumes were repeated until the last two measurements had standard deviations smaller than 0.01%.

Water content, bulk density, grain density, dry density, porosity, and void ratio were determined following the procedures outlined in Blum (1997). The pycnometer was calibrated during each measurement run against a sphere of known volume. Mass data were output in grams for convenience, and density data were output as grams per cubic centimeter.

DOWNHOLE LOGGING

Introduction

Downhole logs can be used to determine physical, chemical, and structural properties of formations penetrated by a drill hole. Wireline log data are rapidly collected using a variety of instruments to make continuous in situ measurements as a function of depth below the seafloor after the hole has been drilled or reentered. Logs are essential to determine the borehole stratigraphy at a scale that links laboratory measurements on core samples with regional geophysical studies. After processing, logs also provide information regarding the physical state of the borehole and the character of the formations penetrated.

Principles and Uses of the Tools

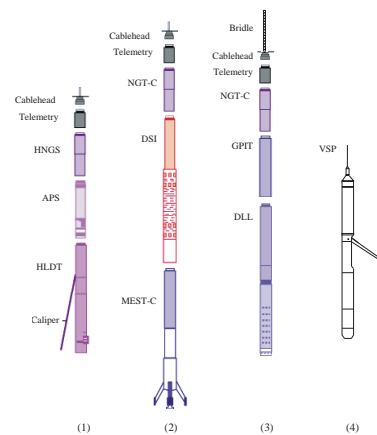
The principles, operation, and uses of the tools are described in Serra (1984, 1986) and Rider (1996). Standard ODP logging tools, applications, and principles for marine geology and geophysics are described by Goldberg (1997) and in previous ODP *Initial Reports* (e.g. Eberli, Swart, Malone, et al., 1997). They are briefly summarized below, and the tool string configurations are shown in Figure F10.

The natural gamma-ray tool (NGT) and hostile environment natural gamma-ray sonde (HNGS) measure the natural gamma radiation from isotopes of potassium, thorium, and uranium in the formation surrounding the tool.

The accelerator porosity sonde (APS) emits fast neutrons, which are slowed by hydrogen in the formation, and the energy of rebounded neutrons is measured. In sediments, most hydrogen is in the pore water and, hence, porosity may be derived. However, in igneous and metamorphic rocks most of the tool response is due to hydrogen in fluids filling fractures and bound in alteration minerals.

The hostile environment litho-density tool (HLDT) emits high-energy gamma rays, which are scattered by the electrons in the formation. The electron density (and hence bulk density) is derived from the

F10. Schematic diagram of Dipole Sonic Imager, p. 37.



energy of the returning gamma rays. Porosity may also be derived from bulk density, if the matrix density is known. In addition, the photoelectric effect (PEF) is measured, and this varies according to the chemical composition of the formation. The HLDT, APS, and HNGS were first used by ODP during Leg 166 (Eberli, Swart, Malone, et al., 1997).

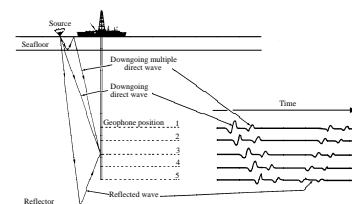
The dual laterolog (DLL) tool measures the formation resistivity at two different penetration depths by measuring the intensity of a variable current flowing from an electrode to a remote return. This intensity is proportional to the formation's electrical conductivity. Two symmetrical guard electrodes emit focusing currents constraining the current beam to flow perpendicularly out into the formation and coaxially with the tool. The deep current (LLd) is focused in a path ~0.6 m wide that flows back to the surface while achieving deep penetration into the formation and reducing the borehole effect. For the shallow measurement (LLs), the same current electrode is used at a different frequency for measuring and focusing currents for the LLs return to electrodes located within the tool. This restricts the measurement to a shallower region. Definition of lithologic units, as well as estimation of total and fracture porosity, are often obtained from DLL measurements.

The Dipole Sonic Imager (DSI) employs a combination of monopole and dipole transducers to make accurate measurements of sonic wave propagation in a wide variety of lithologies (Schlumberger, 1995). In addition to high-quality compressional wave velocity measurements, the DSI excites a flexural mode in the borehole that can be used to determine shear-wave velocity in all types of formations. The configuration of the DSI also allows recording of cross-line dipole waveforms that can be used to estimate shear-wave splitting caused by preferred mineral and/or structural orientations in consolidated formations. A low-frequency source enables Stoneley waveforms to be acquired as well.

The Formation MicroScanner (FMS) produces high-resolution images of the microresistivity character of the borehole wall. The tool is comprised of four orthogonal pads, each having 16-button electrodes that are pressed against the borehole wall (Serra, 1989). Roughly 30% of a 25-cm diameter borehole is imaged. The vertical resolution is ~5 mm, which allows features such as thin units, fractures, and veins to be imaged. A three-component magnetometer within the general-purpose inclinometry tool (GPIT) is part of the FMS tool configuration and allows the images to be oriented with respect to true geographical north. Hence, directional structure information can be obtained for unit boundaries, faults, and foliations.

Vertical seismic profile (VSP) experiments measure compressional-wave velocities in situ in the seafloor where it is intersected at the borehole from direct waves at seismic frequencies (10–100 Hz) and at seismic scales (hundreds of meters). The experiment provides results intermediate between small-scale measurements such as laboratory analysis of cores and sonic logs and large-scale measurements such as seismic refraction and reflection. During a VSP, a borehole seismometer is clamped successively at different depths in the borehole (Fig. F11; Hardage, 1983; Balch and Lee, 1984; Gal'perin, 1974). Seismic sources such as air guns and water guns are fired next to the ship, and the borehole seismometer records both the direct, downgoing waves and upgoing waves reflected from changes in acoustic impedance below the receiver. Interval velocities are computed from the difference in arrival time of the direct wave between different receiver depths. An excellent review of VSP methodology as carried out on *JOIDES Resolution* is given in Shipboard Scientific Party (1989; pp. 182–199). Processing tech-

F11. Schematic diagram of VSP geometry, p. 38.



niques can be applied to separate the upgoing and downgoing wavefields (Ross and Shaw, 1987; Christie et al., 1983; Kommedal and Tjostheim, 1989), which can then be analyzed for the attenuation properties of rock (Rutledge and Winkler, 1989; Swift and Stephen, 1992), for prediction of acoustic properties below the bottom of the hole (Swift et al., 1991) and for correlation with borehole lithology, wireline logs, and events on conventional seismic reflection and refraction profiles (Bolmer et al., 1992). Resolution of structure is limited by the signal-to-noise ratio, bandwidths of the source and receiver, and rock velocities. In marine use, the frequency of the source ranges from 5–30 Hz for explosives and large air guns to ~120 Hz for water guns. In rocks having velocities from 4 to 8 km/s, the finest scales resolvable (about one-quarter of a wavelength) with a broadband receiver under good signal-to-noise conditions are 8–200 m. Previous DSDP and ODP VSP experiments are described in Stephen (1979), Duennebier et al. (1987), and Shipboard Scientific Party (1995c).

Data Quality

Data quality is largely determined by the state of the borehole wall. If it is irregular, wide, or has many washouts, there are problems with the tools that require good contact with the wall (density, porosity, and FMS). However, deep investigative measurements, such as resistivity and sonic velocity, are less sensitive to variations in the hole diameter.

Operations

During Leg 176, Hole 735B was reentered and logged using two different wireline tool strings at the beginning of the leg and four tool strings at the end (Fig. F10), after coring and fishing operations were concluded. The wireline tool strings combined standard ODP tools with two new tools, the DSI and the Schlumberger BGKT three-component VSP tool. The wireline tools and the shipboard MAXIS unit, which recorded and monitored the log data acquisition in real time, were provided by Schlumberger. The Lamont-Doherty Earth Observatory Borehole Research Group (LDEO-BRG) active wireline heave compensator was used during the logging operations to minimize the effects of the ship's motion during each of the logging runs. The LDEO-BRG memory temperature logging tool was also used to record in situ borehole temperatures. After the logs were acquired, the data were transferred to the shipboard Downhole Measurements Laboratory for preliminary interpretation using the Geoframe software package and also to the LDEO-BRG for processing using the SeaNET high-speed satellite data link.

Dipole Sonic Imager

The deployment of the DSI during Leg 176 consisted of two passes with the FMS-sonic tool string, where the DSI replaced the commonly used array sonic tool (SDT). Two passes are required to obtain consistent azimuth measurements for the cross-dipole mode and to acquire additional recording modes at normal logging speeds. Switching of recording modes was accomplished while the tool was downhole and in the same manner as it was performed during ODP Leg 174B (Becker, Malone, et al., 1998). The DSI was run first using the conventional *P*-wave first arrival, in-line dipole, and cross-dipole recording modes; then

subsequently using the Stoneley-wave, high-frequency *P*-wave, *S*-wave, and cross-dipole recording modes.

Vertical Seismic Profile

Leg 176 was the first to use the Schlumberger three-component VSP tool (Fig. F10). This tool has been used for many years in the petroleum exploration industry and is supported by the Schlumberger logging engineer on board *JOIDES Resolution*.

To measure the far-field incident wavefield in the water column, we also deployed an over-the-side hydrophone at a depth of 200–300 m. This hydrophone is separate from the blast phone on the guns. The blast phone measures the initial blast of the gun and is used as the start time for seismic recording. The over-the-side hydrophone measures the true amplitude pressure waveform in the far field (at least a wavelength or two from the source). It includes the interference effect of the free surface above the guns. Monitoring during the VSP experiment is important for amplitude and waveform studies such as reflectivity modeling and attenuation analysis. Significant amplitude, waveform, and frequency changes can occur during the experiment because of small variations in depth or air pressure.

The Leg 176 VSP was planned (1) to provide seismic interval velocities with which the rock sequence intersected by the borehole could be compared, (2) to place the borehole results in their proper setting with respect to the seismically defined structure of the oceanic crust and mantle, (3) to estimate the degree of large-scale fracturing (>0.5 m) by comparing seismic interval velocities with velocities measured in the laboratory on core samples and measured in situ by sonic logging, (4) to correlate borehole lithology with the upgoing seismic reflected wavefield, (5) to predict structure and lithology changes below the drill hole, and (6) to estimate physical properties of rock on seismic scales by studying particle motion and downhole seismic attenuation.

Core Imaging

The principal objectives of the core imaging project were (1) to provide a comprehensive set of digital core images, including both unrolled 360° and slabbed images, recorded using the DMT Digital Color CoreScan system, (2) to identify and measure planar features on unrolled images for comparison to core structural analysis and integration with geographically oriented FMS images, and finally, (3) to match and reorient core images and structural data to true geographic north obtained from the GPIT on the FMS tool string.

The DMT Color CoreScan system is a portable core-imaging unit that was used for the first time on board *JOIDES Resolution* during Leg 173 (Whitmarsh, Beslier, Wallace, et al., 1998). Images were recorded on both slabbed and full-round core surfaces using a 24-bit, three-color (red, green, and blue) CCD line-scan camera with a resolution of 5184 pixels/m (131 pixels/in) and a spectral response between 400 and 700 nm. In the unrolled mode, whole-round core is rotated around its cylindrical axis with the camera line scan positioned parallel to the axis of rotation. Unrolled images as much as 1 m long are recorded in 33-cm sections that are integrated and light calibrated using the DMTGrab Software (DMT CoreScan Users Manual, 1996). Whole-round cores in the unrolled mode are scanned at a rate of ~1.20 min/m, which creates a 14-MB bitmap file. Split archive-half core images as long as 1 m are

recorded in slabbed mode with the camera line scan traveling perpendicular to the vertical core axis. Scanning 1 m of split core takes ~45 s and creates a 10-MB bitmap file.

During Leg 176, all cores were scanned in the unrolled mode with the exception of those pieces that were not fully cylindrical and intervals of drilling breccia. Whole-round cores were scanned after the core was run through the MST. A vertical line marked on the core with a red grease pencil aided initial reorientation of the images back to the ODP reference frame. Unrolled images were obtained on contiguous core pieces whenever possible. The lengths of whole-round pieces unsuitable for scanning were measured so the allowance could be made for them when images were integrated into core barrel lengths using the DMT Software CoreLog (DMT CoreScan Users Manual, 1996). Initial structural analysis was performed; however, the majority of the structural analysis and core reorientation work was done after the cruise. During our sail to Hole 735B, split core (slabbed) images of the archive-half were obtained from the bottommost 50 m of the hole cored during Leg 118. Selected images of the working half were also obtained from new cores during Leg 176.

REFERENCES

- Balch, A.H., and Lee, M.W. (Eds.), 1984. *Vertical Seismic Profiling: Techniques, Applications, and Case Histories*: Boston (Int. Human Resour. Develop. Corp.).
- Becker, K., Malone, M., et al., 1998. *Proc. ODP, Init. Repts.*, 174B: College Station, TX (Ocean Drilling Program).
- Blum, P., 1997. Physical Properties Handbook: a Guide to the Shipboard Measurements of Physical Properties of Deep-Sea cores. *ODP Tech. Note*, 26. College Station, TX (Ocean Drilling Program).
- Bolmer, S.T., Buffler, R.T., Hoskins, H., Stephen, R.A., and Swift, S.A., 1992. Vertical seismic profile at Site 765 and seismic reflectors in the Argo Abyssal Plain. In Gradstein, F.M., Ludden, J.N., et al., *Proc. ODP, Sci. Results*, 123: College Station, TX (Ocean Drilling Program), 583–600.
- Bouchez, J.L., et al., 1992. Submagmatic microfractures in granite. *Geology*, 20:456–459.
- Boyce, R.E., 1976. Definitions and laboratory techniques of compressional sound velocity parameters and wet-water content, wet-bulk density, and porosity parameters by gravimetric and gamma-ray attenuation techniques. In Schlanger, S.O., Jackson, E.D., et al., *Init. Repts. DSDP*, 33: Washington (U.S. Govt. Printing Office), 931–958.
- Cannat, M., Mével, C., and Stakes, D., 1991. Normal ductile shear zones at an oceanic spreading ridge: tectonic evolution of Site 735 gabbros (southwest Indian Ocean). In Von Herzen, R.P., Robinson, P.T., et al., *Proc. ODP, Sci. Results*, 118: College Station, TX (Ocean Drilling Program), 415–429.
- Christie, P.A.F., Hughes, V.J., and Kennett, B.L.N., 1983. Velocity filtering of seismic reflection data. *First Break*, 1:9–24.
- Dick, H.J.B., Meyer, P.S., Bloomer, S., Kirby, S., Stakes, D., and Mawer, C., 1991a. Lithostratigraphic evolution of an in-situ section of oceanic Layer 3. In Von Herzen, R.P., Robinson, P.T., et al., *Proc. ODP, Sci. Results*, 118: College Station, TX (Ocean Drilling Program), 439–538.
- Dick, H.J.B., Schouten, H., Meyer, P.S., Gallo, D.G., Bergh, H., Tyce, R., Patriat, P., Johnson, K.T.M., Snow, J., and Fisher, A., 1991b. Tectonic evolution of the Atlantis II Fracture Zone. In Von Herzen, R.P., Robinson, P.T., et al., *Proc. ODP, Sci. Results*, 118: College Station, TX (Ocean Drilling Program), 359–398.
- DMT-GeoTec/Geo-Engineering, 1996. *DMT Color CoreScan Users Manual. Acquisition and Evaluation Software*.
- Duennebier, F.K., Lienert, B., Cessaro, R., Anderson, P., and Mallick, S., 1987. Controlled-source seismic experiment at Hole 581C. In Duennebier, F.K., Stephen, R., et al., *Init. Repts. DSDP*, 88: Washington (U.S. Govt. Printing Office), 105–125.
- Eberli, G.P., Swart, P.K., Malone, M.J., et al., 1997. *Proc. ODP, Init. Repts.*, 166: College Station, TX (Ocean Drilling Program).
- Gal'perin, E.I., 1974. *Vertical Seismic Profiling*. Spec. Publ.—Soc. Explor. Geophys., 12.
- Gerland, S., and Villinger, H., 1995. Nondestructive density determination on marine sediment cores from gamma-ray attenuation measurements. *Geo-Mar. Lett.*, 15:111–118
- Goldberg, D., 1997. The role of downhole measurements in marine geology and geophysics. *Rev. Geophys.*, 315–342.
- Hardage, B.A., 1983. *Vertical Seismic Profiling: Part A, Principles*: London (Geophysical Press).
- Hirth, G., and Kohlstedt, D.L., 1995. Experimental constraints on the dynamics of the partially molten upper mantle: deformation in the diffusion creep regime. *J. Geophys. Res.*, 100:1981–2001.
- Hoppie, B.W., Blum, P., and the Shipboard Scientific Party, 1994. Natural gamma-ray measurements on ODP cores: introduction to procedures with examples from Leg

150. In Mountain, G.S., Miller, K.G., Blum, P., et al., *Proc. ODP, Init. Repts.*, 150: College Station, TX (Ocean Drilling Program), 51–59.
- Kommedal, J.H., and Tjøstheim, B.A., 1989. A study of different methods of wavefield separation for application to VSP data. *Geophys. Prospect.*, 37:117–142.
- Le Maitre, R.W., 1989. *A Classification of Igneous Rocks and Glossary of Terms*: Oxford (IUGS, Blackwell).
- Means, W.D., and Park, Y., 1994. New experimental approach to understanding igneous texture. *Geology*, 22:323–326.
- Mons, R., and Barbour, K., 1981. Vertical seismic profiling. *Schlumberger Wireline Atlantic-Marketing Geophys.*, SMP-1108.
- Nicolas, A., and Ildefonse, B., 1996. Flow mechanisms and viscosity in basaltic magma chambers. *Geophys. Res. Lett.*, 23:2013–2016.
- Rider, M., 1996. *The Geological Interpretation of Well Logs*: Caithness (Whittles Publishing).
- Ross, W.S., and Shaw, P.M., 1987. Vertical seismic profile reflectivity: ups over downs. *Geophysics*, 52:1149–1154.
- Rutledge, J.T., and Winkler, H., 1989. Attenuation measurements from vertical seismic profile data: Leg 104, Site 642. In Eldholm, O., Thiede, J., Taylor, E., et al., *Proc. ODP, Sci. Results*, 104: College Station, TX (Ocean Drilling Program), 965–972.
- Schlumberger, 1995. *DSI—Dipole Sonic Imager*: (Schlumberger Wireline and Testing), SMP-5128.
- Serra, O., 1984. *Fundamentals of Well-Log Interpretation* (Vol. 1): *The Acquisition of Logging Data*: Dev. Pet. Sci., 15A: Amsterdam (Elsevier).
- , 1989. *Formation MicroScanner Image Interpretation*: Houston (Schlumberger Educ. Services), SMP-7028.
- , 1986. *Fundamentals of Well-Log Interpretation* (Vol. 2): *The Interpretation of Logging Data*. Dev. Pet. Sci., 15B.
- Shafer, H.N.S., 1996. The determination of iron(II) oxide in silicate and refractory materials. Part II. *The Analyst*, 91:755–762.
- Shipboard Scientific Party, 1989. Site 735. In Robinson, P.T., Von Herzen, R., et al., *Proc. ODP, Init. Repts.*, 118: College Station, TX (Ocean Drilling Program), 89–222.
- , 1991. Explanatory notes. In Taira, A., Hill, I., Firth, J.V., et al., *Proc. ODP, Init. Repts.*, 131: College Station, TX (Ocean Drilling Program), 25–60.
- , 1992. Explanatory notes. In Dick, H.J.B., Erzinger, J., Stokking, L.B., et al., *Proc. ODP, Init. Repts.*, 140: College Station, TX (Ocean Drilling Program), 5–33.
- , 1993. Explanatory notes. In Gillis, K., Mével, C., Allan, J., et al., *Proc. ODP, Init. Repts.*, 147: College Station, TX (Ocean Drilling Program), 15–42.
- , 1995a. Explanatory notes. In Cannat, M., Karson, J.A., Miller, D.J., et al., *Proc. ODP, Init. Repts.*, 153: College Station, TX (Ocean Drilling Program), 15–42.
- , 1995b. Explanatory notes. In Humphris, S.E., Herzig, P.M., Miller, D.J., et al., *Proc. ODP, Init. Repts.*, 158: College Station, TX (Ocean Drilling Program), 37–53.
- , 1995c. Explanatory notes. In Shipley, T.H., Ogawa, Y., Blum, P., et al., *Proc. ODP, Init. Repts.*, 156: College Station, TX (Ocean Drilling Program), 39–68.
- , 1998. Explanatory notes. In Fouquet, Y., Zierenberg, R., Miller, D.J., et al., *Proc. ODP, Init. Repts.*, 169: College Station, TX (Ocean Drilling Program), 17–32.
- Stephen, R.A., 1979. The oblique seismic experiment in oceanic crust: experiment and technique. *Mar. Geophys. Res.*, 4:213–226.
- Streckeisen, A., 1974. Classification and nomenclature of plutonic rocks. *Geol. Rundsch.*, 63:773–786.
- Swift, S.A., Hoskins, H., and Stephen, R.A., 1991. Seismic stratigraphy in a transverse ridge, Atlantis II Fracture Zone. In Von Herzen, R.P., Robinson, P.T., et al., *Proc. ODP, Sci. Results*, 118: College Station, TX (Ocean Drilling Program), 219–226.
- Swift, S.A., and Stephen, R.A., 1992. How much gabbro is in ocean seismic layer 3? *Geophys. Res. Lett.*, 19:1871–1874.
- Whitmarsh, R.B., Beslier, M.-O., Wallace, P.J., et al., 1998. *Proc. ODP, Init. Repts.*, 173: College Station, TX (Ocean Drilling Program).

Figure F1. Diagram illustrating terms used in the discussion of coring operations and core recovery.

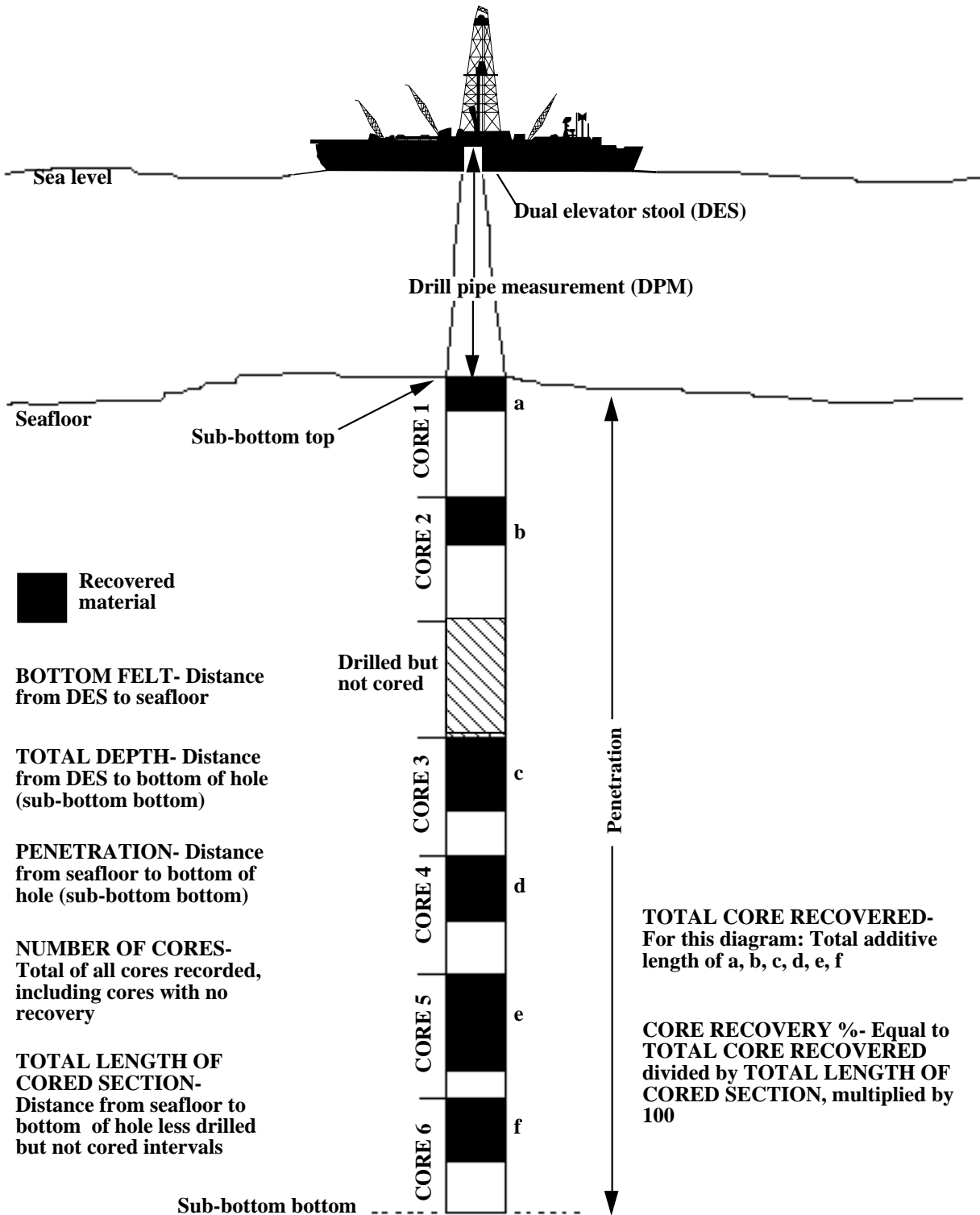


Figure F2. Diagram illustrating hard-rock core division procedures.

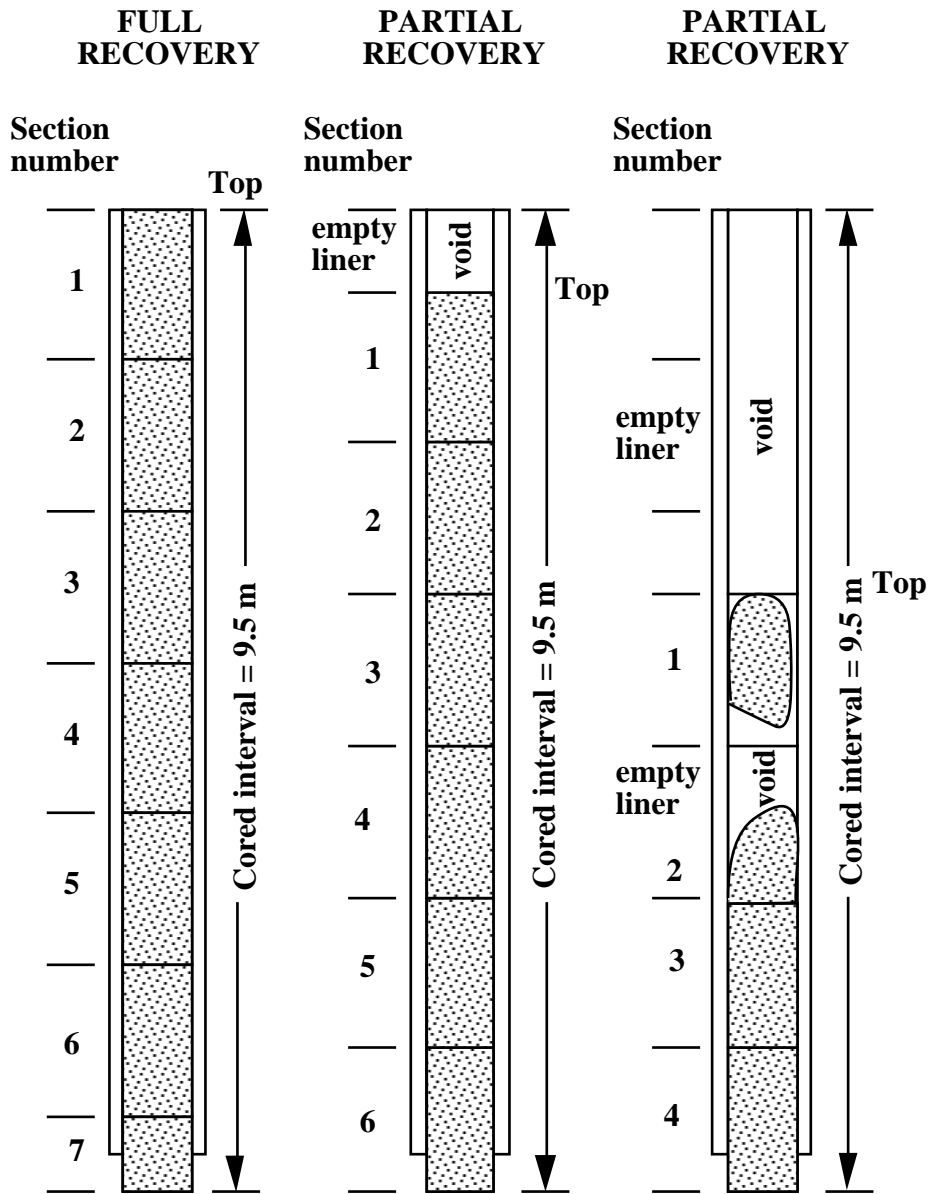


Figure F3. This figure illustrates core curation procedures for hard rocks. Letters designating pieces as removed from core barrel are for illustrative purposes only. Pieces A, B, C, D, E, and F become interval XXX-YYYY-1R-1, Piece 1 to Piece 6 (where XXX is the leg, YYY is the site, and Z is the hole designator). Because pieces G and H can be reoriented to fit along a fracture, they are curated as a single piece. In this case, the reassembled single piece is too long to fit in the bottom of Section 1R-1, so it is shunted to the top of Section 1R-2 and curated as interval XXX-YYYY-1R-2, (Pieces 1A and 1B). Similarly, pieces L and M are too long to fit in the bottom of Section 1R-2 after realignment and are shunted to the top of Section 1R-3. Spacers between pieces also artificially add length to the core when measured for archiving and curation. For example, pieces L and M represent an interval from 2.17 to 2.63 m down from the top of the core as removed from the core barrel, but are archived as interval XXX-YYYY-1R-3 (Pieces 1A and 1B, 0.0–46.0 cm).

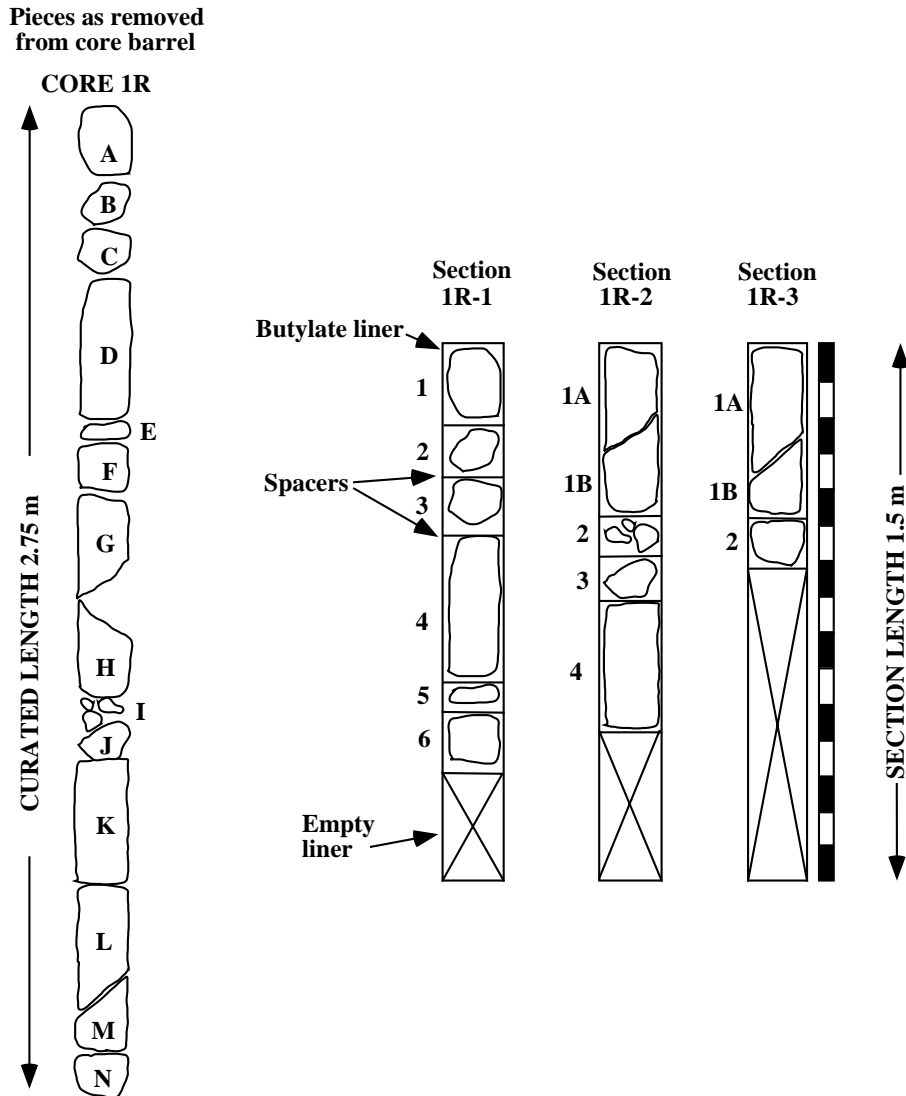


Figure F4. Example of hard-rock visual core description (HRVCD) form.

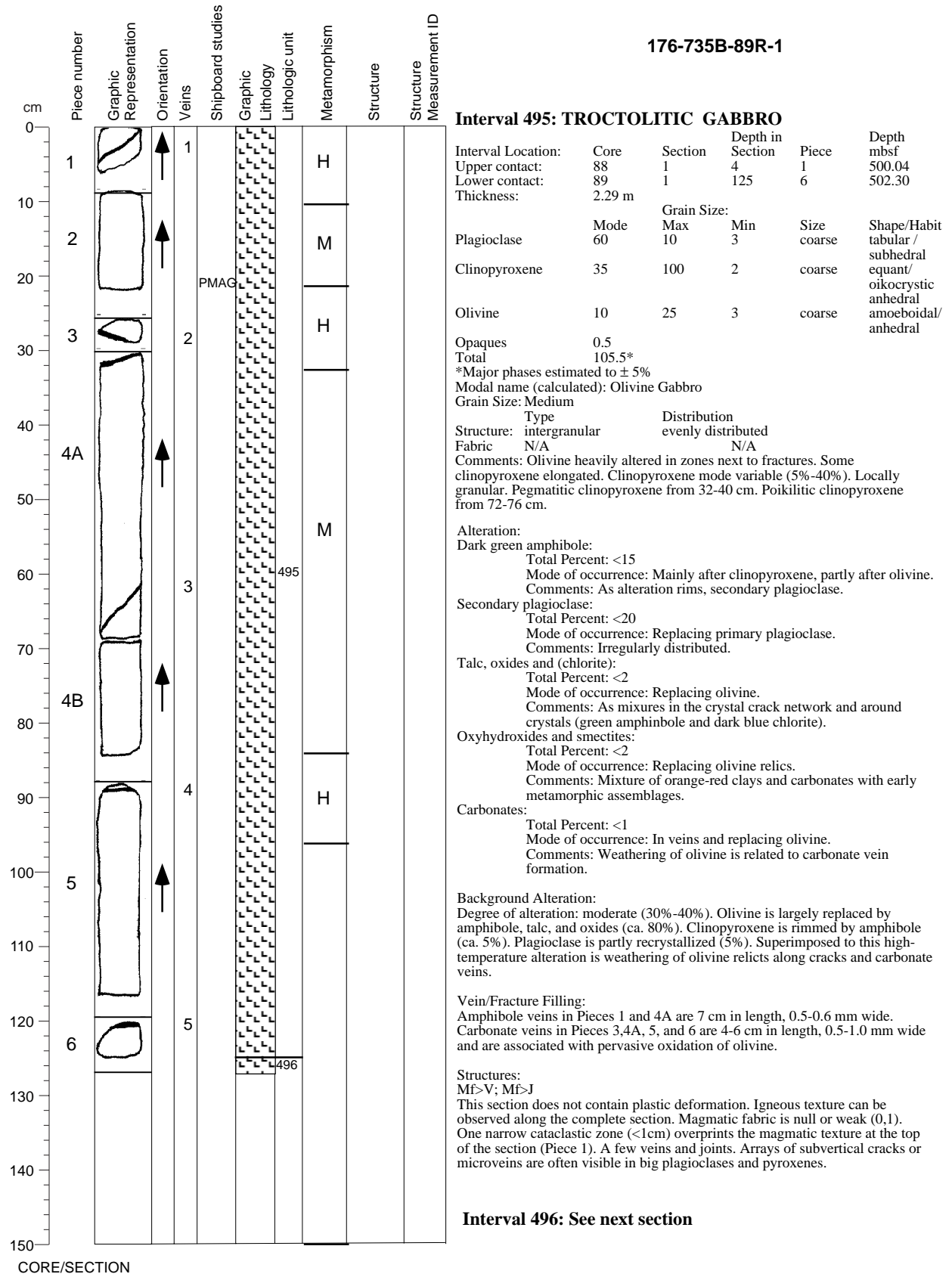


Figure F5. Graphic lithology patterns used during Leg 176.



Gabbro



Microgabbro



Oxide gabbro



Troctolite



Olivine gabbro



Oxide troctolite



Oxide olivine gabbro



Diorite



Gabbronorite



Clinopyroxenite



Oxide gabbronorite

Figure F6. Comparison of lithostratigraphic intervals defined during Leg 176 with those defined by Dick et al. (1991a) for the core recovered from 450 to 500 mbsf during Leg 118.

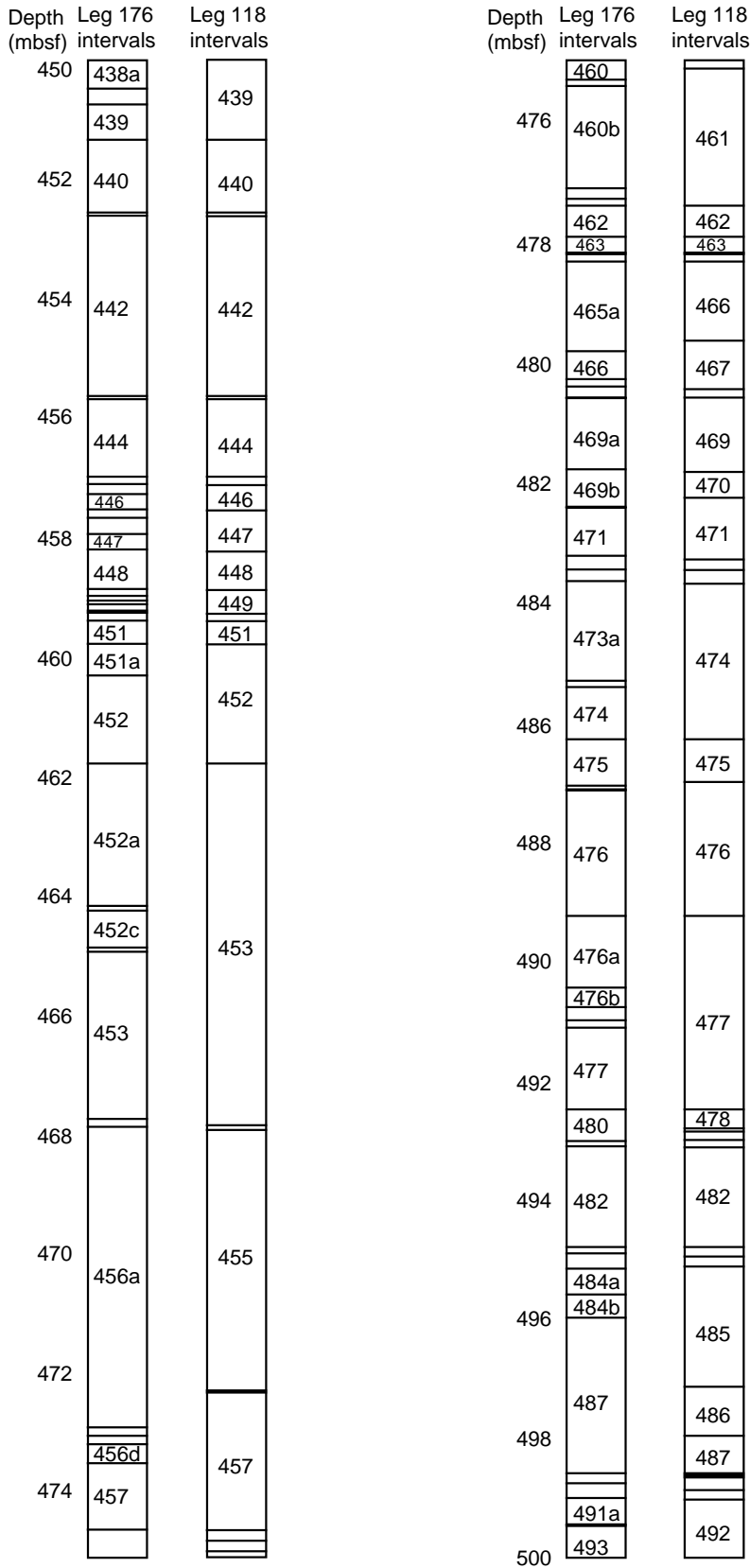


Figure F7. Classification of ultramafic and gabbroic rocks composed of olivine, clinopyroxene, orthopyroxene, and plagioclase (after Streckeisen, 1974).

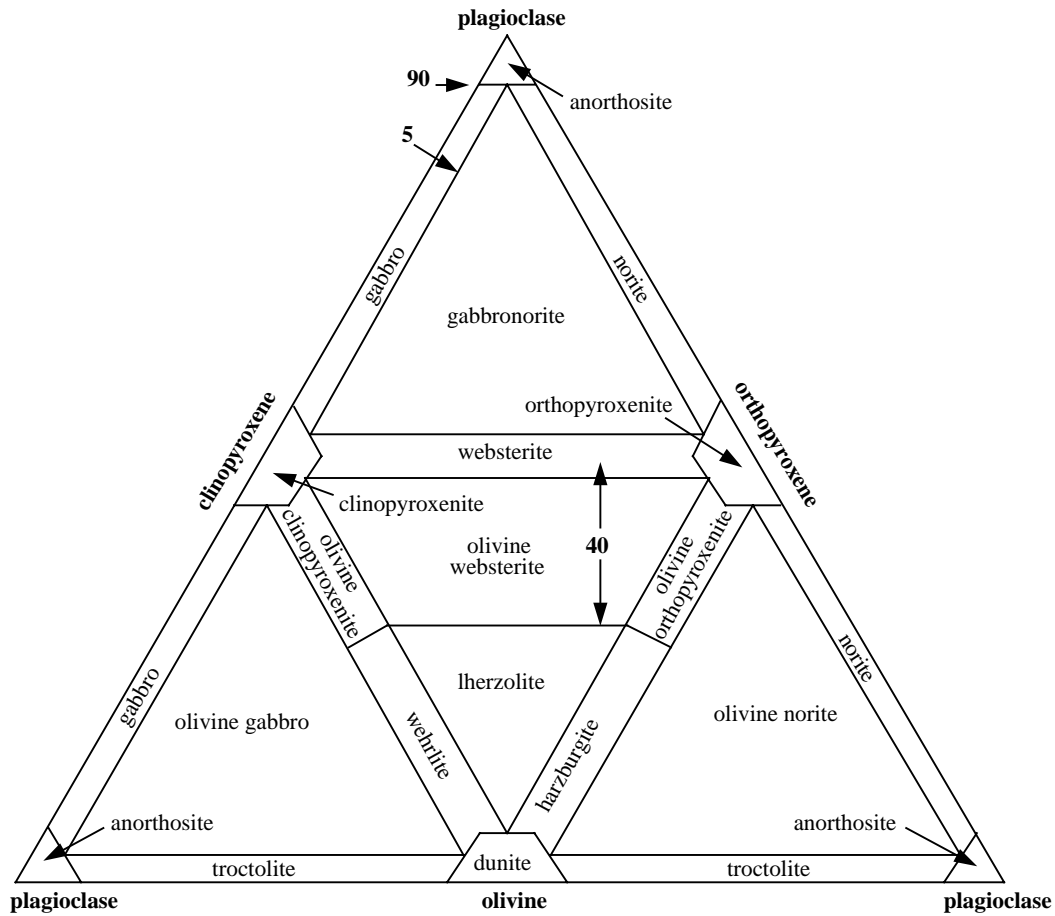


Figure F8. Classification of silica saturated or oversaturated plutonic rocks, based on quartz, plagioclase, and alkali feldspar (Streckeisen, 1974).

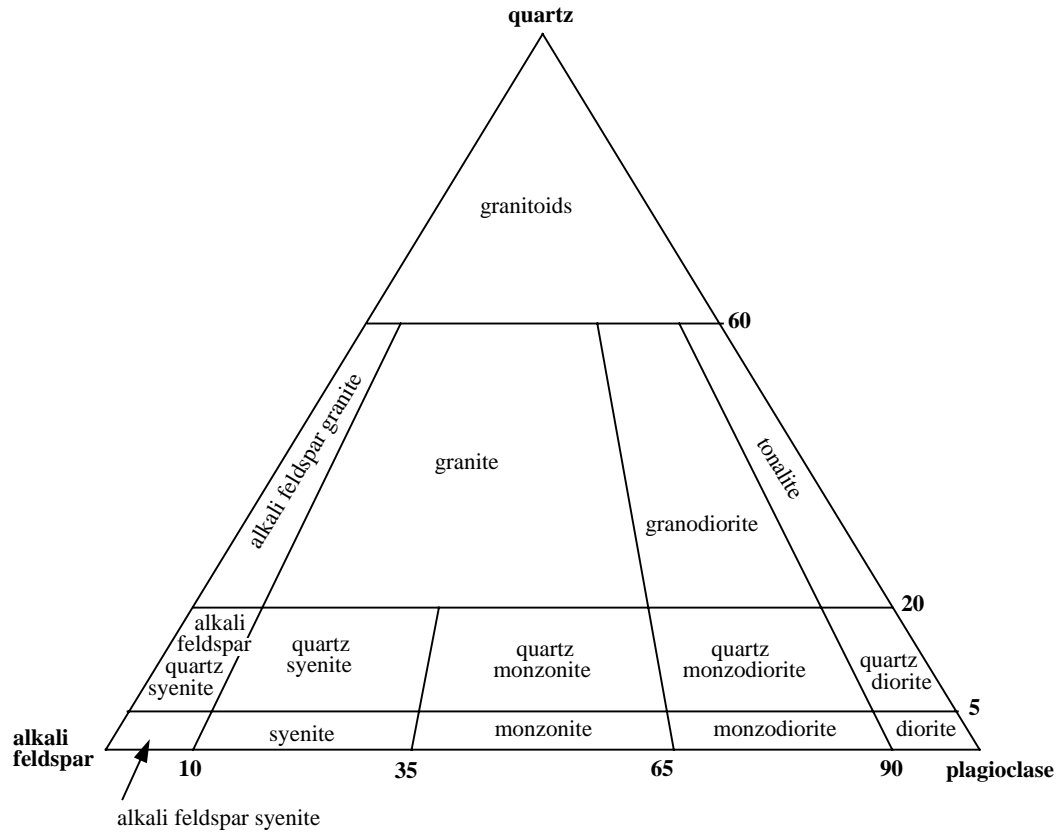
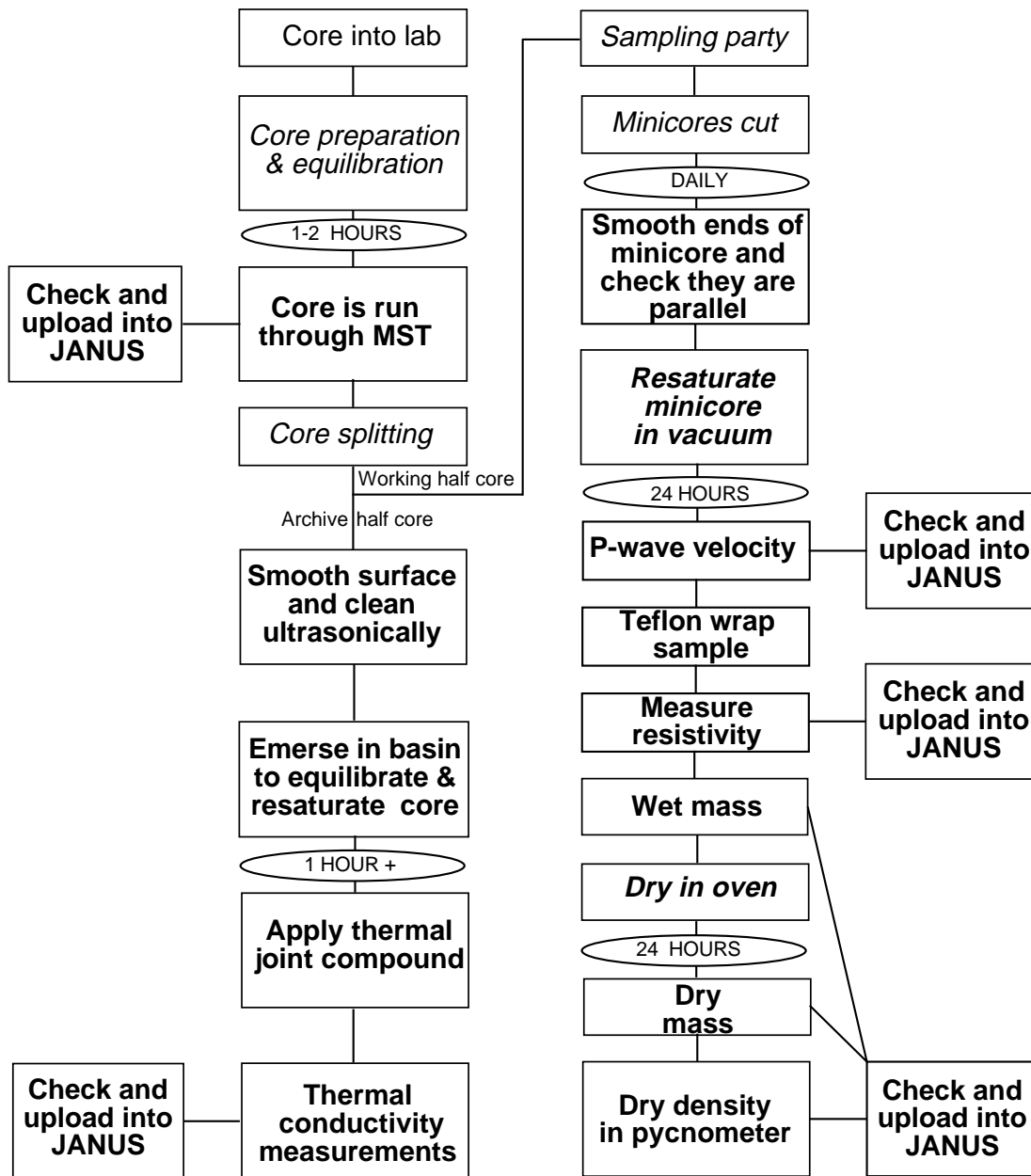


Figure F9. Core flow for physical properties measurements in hard-rock boreholes.



ITALICS = Time lags

BOLD = PHYSICAL PROPERTY TEAM ACTIONS

Figure F10. Schematic diagram of the wireline logging tool strings deployed during Leg 176. (1) Modified triple combo string deployed at the end of the cruise; (2) FMS/DSI combination; (3) resistivity (DLL) and general purpose inclinometry tool (GPIT) combination; and (4) VSP tool.

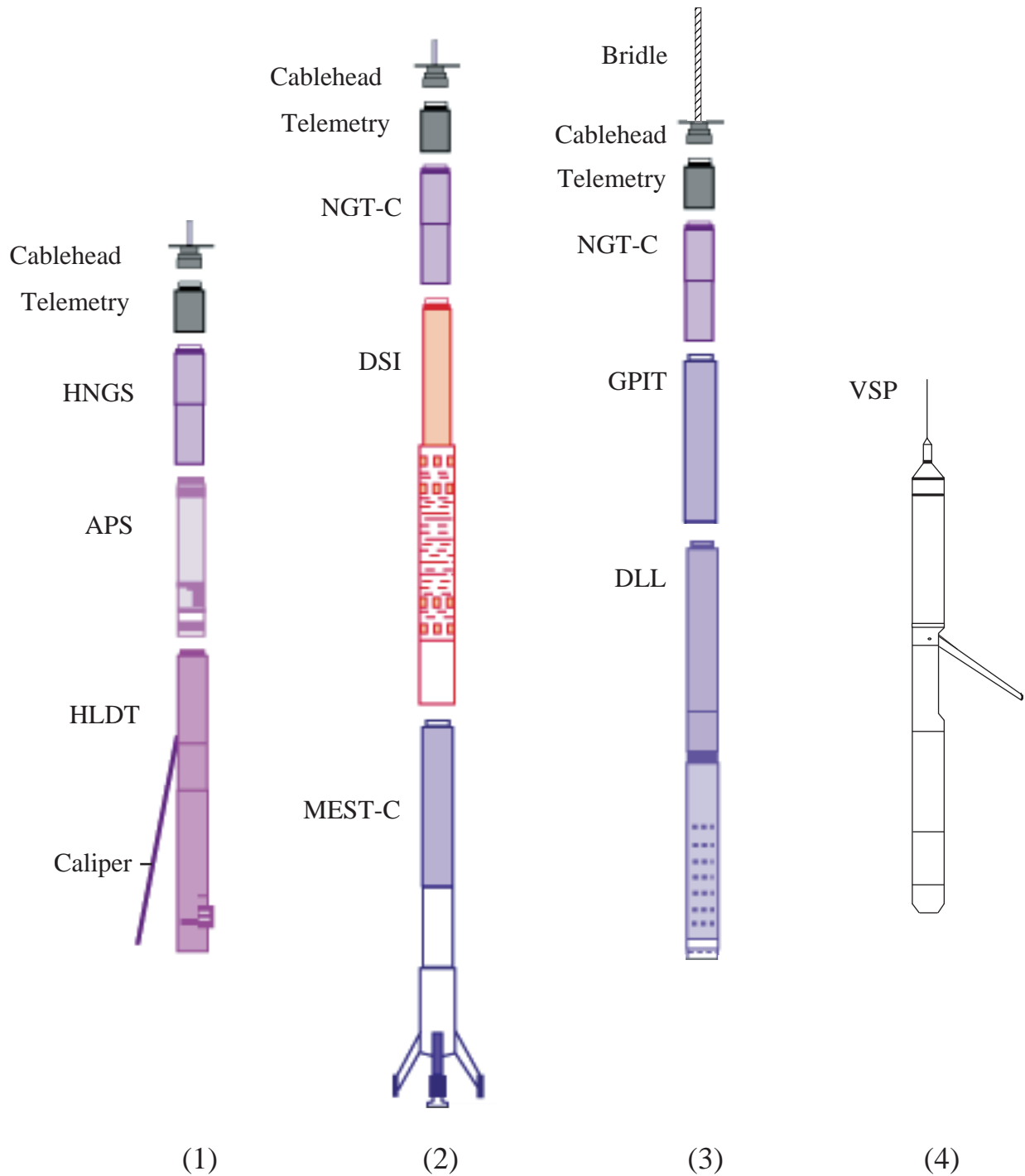


Figure F11. Schematic diagram of VSP geometry and record section illustrating how direct and reflected arrivals differ with changes in receiver depth (modified after Mons and Barbour, 1981).

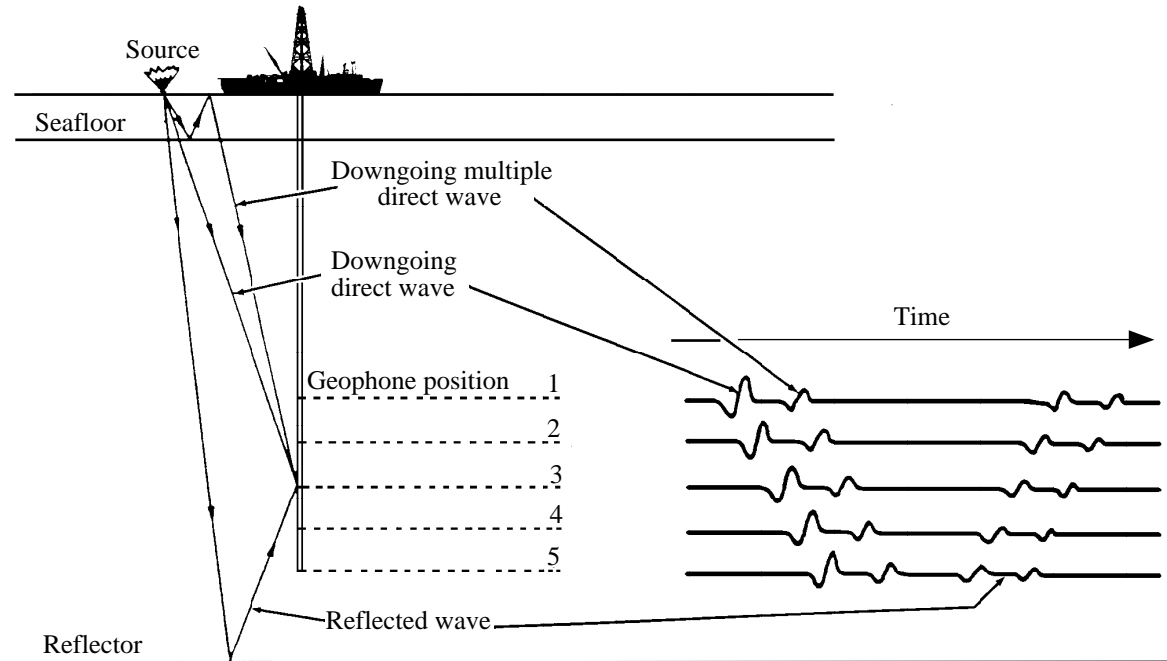


Table T1. X-ray fluorescence operating conditions.

Oxide or element	Line	Crystal	Detector	Collimator	Peak angle (°2θ)	Background offset (°2θ)	Count time on peak (s)	Count time on background (s)
SiO ₂	Kα	PET	FPC	Medium	109.21		40	
TiO ₂	Kα	LIF200	FPC	Fine	86.14		40	
Al ₂ O ₃	Kα	PET	FPC	Medium	145.12		100	
Fe ₂ O ₃	Kα	LIF200	FPC	Fine	57.52		40	
MnO	Kα	LIF200	FPC	Fine	62.97		100	
MgO	Kα	TLAP	FPC	Medium	45.17	±0.80	150	150
CaO	Kα	LIF200	FPC	Medium	113.09		40	
Na ₂ O	Kα	TLAP	FPC	Medium	54.10	-1.20	150	150
K ₂ O	Kα	LIF200	FPC	Medium	136.69		100	
P ₂ O ₅	Kα	GE111	FPC	Medium	141.04		100	
Rh	Kα Compton	LIF200	Scint	Fine	18.58		60	
Nb	Kα	LIF200	Scint	Fine	21.40	+0.35	200	100
Zr	Kα	LIF200	Scint	Fine	22.55	-0.35	100	50
Y	Kα	LIF200	Scint	Fine	23.80	-0.40	100	50
Sr	Kα	LIF200	Scint	Fine	25.15	-0.40	100	50
Rb	Kα	LIF200	Scint	Fine	26.62	-0.60	100	50
Zn	Kα	LIF200	Scint	Medium	41.81	-0.55	100	50
Cu	Kα	LIF200	Scint	Fine	45.03	-0.55	100	50
Ni	Kα	LIF200	Scint	Medium	48.67	-0.60	100	50
Cr	Kα	LIF200	FPC	Fine	69.35	-0.50	100	50
V	Kα	LIF220	FPC	Fine	123.06	-0.50	100	50

Notes: All major elements measured using a rhodium X-ray tube operated at 30 kV and 80 mA. Trace elements are measured using a rhodium X-ray tube operated at 60 kV and 50 mA. Detector: FPC = flow proportional counter (P10 gas); Scint = NaI Scintillation counter. Detection limits in weight percent for major oxides, parts per million for trace elements.

Table T2. Deformation intensity scales.

Category:	0	1	2	3	4	5
Magmatic	Isotropic: no shape fabric	Weak shape fabric	Moderate shape fabric	Strong shape fabric		
Crystal plastic	Undeformed	Weakly foliated	Strongly foliated	Porphyroclastic (proto)mylonite	Mylonite	Ultramylonite
Cataclastic	Undeformed	Minor fracturing: no significant grain-size reduction	Moderate fracturing: no significant grain-size reduction	Dense anastomosing fracturing and incipient breccia (<20% matrix)	Well-developed fault brecciation; rotation of clasts (20% to 70% matrix)	Cataclasite (>70% matrix)
Joints	Unfractured	Minor fracturing (≤ 1 per 10 cm)	(1 to 5 per 10 cm)	(>5 per 10 cm)		
Veins	No veins	Occasional veins (= filled fractures) (≤ 1 per 10 cm)	Moderate veining (1 to 5 per 10 cm)	Intense vein networks (>5 per 10 cm)		

Table T3. Checklist used for spreadsheet comments associated with each structural identifier.

The following is a checklist of structural characteristics that were searched for in macroscopic core samples. These characteristics supplement the information required by the spreadsheet and were noted in the comments section of the spreadsheet. The abbreviations for these features were used to document crosscutting relationships (where > indicates "older than") on the structure section of the VCDs.

Subhorizontal microcracks (Shm)
Drilling-induced fractures

Joints (J)
Joint density
Orientation
Plume structures on joint surface

Veins (V)
Orientation of veins and vein-array boundaries
Magnitude and nature of offset
Density of vein network
Array characteristics
Sense of shear
Angle between new vein segments and array boundary (measure of array dilatation)
Internal structure of fibers
Crack-seal structures and number of vein-opening events
Wall-rock alteration and shape
Vein terminations (splayed or tapered)
Vein mineralogy

Faults (F)
Fault-zone thickness, orientation and density
Movement sense (r,n,d,s), reverse, normal, dextral sinistral
Intensity of cataclastic fabric (Cf)
Matrix material (gouge or secondary minerals)
Overprinting of pre-existing fabric
Semi-brittle

Breccias (B)
Hydrothermal (Bh), magmatic (Bm) or cataclastic (Bc)
Clast size and shape, matrix composition, relative proportions

Cleavages (C)
Style of cleavage (e.g., crenulation [Cc], spaced [Cs])
Spacing or wavelength
Angle between cleavage and earlier fabrics, noting directions of larger-scale fold closures

Folds (Fo)
Inter-limb angle
Estimate of hinge curvature (e.g., kink vs. round)
Asymmetry of hingeline relative to other fabrics (e.g., stretching lineations, etc.)
Other geometrical aspects preserved in core (e.g., wavelength, amplitude, etc.)
Number of folds, if more than one

Crystal-Plastic Fabrics (Pf)
Intensity of fabric
Intensity of fabric in retrograde assemblage
Orientation of foliation (Sp) and lineation (Lp)
L-, LS- and S-tectonite
Shear sense indicators: block-rotated porphyroclasts, asymmetric augen, SC fabrics, discrete shear bands, mica-fish, and tension-gash arrays (r,n,d,s), reverse, normal, dextral sinistral
Mineralogical segregation or banding

Magmatic Fabrics (Mf)
Intensity and orientation of foliations (Sm) and lineations (Lm)
Minerals that define the shape and/or crystallographic preferred orientations
Angle between crystallographic and shape fabrics
Orientation of subfabrics

Compositional Layering (Cl)/Gradational Boundaries (Gb)
Type of layering (e.g., sedimentary, igneous cumulate, alteration, etc.)
Orientation, thickness, and density of layers

Igneous Contacts (Ic)
Orientation and density
Concordant or discordant

Crosscutting Relationships
Intrusive relationships, relative chronology of the different fabrics
Angle between compositional layering and magmatic or crystal-plastic fabric

Table T4. Textural types characterized by specific microstructural styles for gabbroic rocks.

Textural group	Plagioclase	Olivine	Pyroxene	Physical state
1	No or minor crystal-plastic deformation microstructures (e.g., deformation twins, undulose extinction)	No deformation microstructures ± local undulose extinction and/or local subgrain development	No deformation microstructures	Primarily magmatic
a	Random shape orientation			
b	Preferred shape orientation			
2	<30% fine-grained recrystallized matrix; deformation twins and subgrain boundaries may be present	Common subgrain boundaries and undulose extinction	No deformation microstructures ± minor crystal-plastic deformation microstructures	Crystal-plastic ± magmatic
3	>30% recrystallized matrix; deformation twins, subgrain boundaries, and undulose extinction common; moderate shape preferred orientation; strong crystallographic preferred orientation	Elongated aggregates of neoblasts	Kinked grains; common to extensive recrystallization	Crystal-plastic
4	Strongly bimodal grain size distribution; localized fine-grained neoblasts, polygonal neoblasts, sutured neoblasts	Closely spaced subgrain boundaries; pervasive undulose extinction extensive neoblasts	Bent/kinked porphyroclasts; localized recrystallization	Crystal-plastic
5	Common intracrystalline microfractures associated with very fine-grained neoblasts; extensive kinked and deformation twinned grains; pervasive undulose extinction; may contain hydrothermal alteration mineral assemblages	Same as plagioclase	Same as plagioclase	Semibrittle
6	Intra/intercrystalline microfractures and cataclastic bands; extensive kinked and deformation twinned grains; pervasive undulose extinction	Same as plagioclase	Same as plagioclase	Brittle/cataclastic